MICROCOPY RESOLUTION TEST CHART
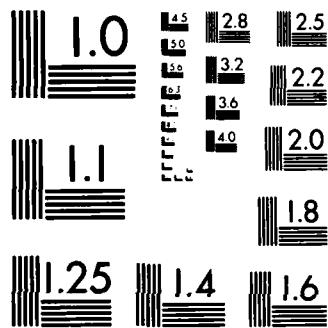
NATIONAL BUREAU OF STANDARDS-1963-A

R&D 3005-MS

GLASS FIBRE/EPOXY RESIN INTERFACE LIFE-TIME PREDICTION

Final Report

by

K H G Ashbee, Principal Investigator
R Hoël
J P Sargent
Elizabeth Walter

United States Army

RESEARCH & STANDARDIZATION GROUP (EUROPE)

London   England

H H Wills Physics Laboratory
University of Bristol
Tyndall Avenue
Bristol BS8 1TL
England

REPORT DOCUMENTATION PAGE		READ INSTRUCTIONS BEFORE COMPLETING FORM
1. REPORT NUMBER	2. GOVT ACCESSION NO.	3. RECIPIENT'S CATALOG NUMBER
4. TITLE *(and Subtitle)* Glass Fibre/Epoxy Resin Interface Life-time Prediction		5. TYPE OF REPORT & PERIOD COVERED Final Technical Report April 1981 – April 1983
		6. PERFORMING ORG. REPORT NUMBER
7. AUTHOR(s) K.H.G. Ashbee, R. Hoël, J.P. Sargent, Elizabeth Walter		8. CONTRACT OR GRANT NUMBER(s) DAJA-37-81-C-0214
9. PERFORMING ORGANIZATION NAME AND ADDRESS H.H. Wills Physics Laboratory University of Bristol Tyndall Avenue, Bristol BS8 1TL, England		10. PROGRAM ELEMENT, PROJECT, TASK AREA & WORK UNIT NUMBERS 6.11.02A 1T16 1102BH57-04
11. CONTROLLING OFFICE NAME AND ADDRESS USARDSG-UK Box 65 FPO New York 09510		12. REPORT DATE April 1983
		13. NUMBER OF PAGES 44
14. MONITORING AGENCY NAME & ADDRESS*(if different from Controlling Office)*		15. SECURITY CLASS. *(of this report)* Unclassified
		15a. DECLASSIFICATION DOWNGRADING SCHEDULE

16. DISTRIBUTION STATEMENT *(of this Report)*

Approved for public release; distribution unlimited

17. DISTRIBUTION STATEMENT *(of the abstract entered in Block 20, if different from Report)*

18. SUPPLEMENTARY NOTES

19. KEY WORDS *(Continue on reverse side if necessary and identify by block number)*

Interfacial pressure pockets. Osmosis. Localised interfacial stress.
Fracture mechanisms of pressure filled cracks. Stress enhanced interfacial
degradation. α-quartz/epoxy interfaces. Kossel X-ray diffraction.
Electron beam back scattering diffraction. Convergent beam diffraction.
Mechanical damping.

20. ABSTRACT *(Continue on reverse side if necessary and identify by block number)*

Load transfer at matrix/fibre interfaces is fundamental to the principle of
fibre reinforcement. The efficiency of load transfer is impaired during
service and one important mechanism for this is osmosis. Water from the
surrounding environment diffuses through the matrix resin, dissolves water
soluble material at the interface and thereby generates osmotic pressure
filled pockets which take the form of cracks propagating into the adjacent
resin.

(cont'd.)

DD $_{1\ JAN\ 73}^{FORM}$ 1473   EDITION OF 1 NOV 65 IS OBSOLETE

S/N 0102-LF-014-6601

It has been demonstrated that osmotic pressure filled cracks in both epoxy and polyester resins are elastic cracks. Use of classical formulae for elastic cracks has enabled estimates to be made of the time dependence of Young's modulus for both resins. Use of linear elastic fracture mechanics formulae has enabled stress intensity factors to be determined from measurements of crack profiles. Radial crack growth rates are small, in the range 10^{-12} ms^{-1} to 10^{-9} ms^{-1} for hot water tests, and remain constant over a wide range of stress intensity factor, from 0.3 to 0.8 MPam$^{1/2}$. Constant radial growth rate is compatible with a diffusion controlled mechanism, and analysis of the data indicates an activation energy of ~50 kcal. Some evidence is presented for concluding that, in polyesters only, the true nature of crack propagation is by way of slip/ stick. The relevance of these findings to in-service interface lifetime prediction is discussed.

Chemical reaction, adsorption and diffusion in polymers are all enhanced by stress and, as is the case for other materials, localised stresses, since they initiate failures, are more important than overall levels of residual stress. The solutions contained inside interfacial pressur pockets are corrosive and their destructive action, on the bonds responsible for load transfer, is enhanced by residual interfacial stress. There exist no high resolution techniques for measuring localised deformation in non-crystalline materials. In crystals, however, local elastic strain can be detected and measured using Kossel X-ray diffraction and electron beam back scattering diffraction in the SEM, and convergent beam diffraction in the TEM. Each of these facilities has been used to study residual stress close to α-quartz/epoxy resin interfaces in order to establish the general nature and magnitude of interfacial stress in SiO_2/epoxy composite materials including GRP. At 40nm from the interface the local strain is ~2%. The corresponding large interfacial stresses are held responsible for the observed very strong dependence of mechanical damping on interfacial area.

ABSTRACT

Load transfer at matrix/fibre interfaces is fundamental to the principle of fibre reinforcement. The efficiency of load transfer is impaired during service and one important mechanism for this is osmosis. Water from the surrounding environment diffuses through the matrix resin, dissolves water soluble material at the interface and thereby generates osmotic pressure filled pockets which take the form of cracks propagating into the adjacent resin.

It has been demonstrated that osmotic pressure filled cracks in both epoxy and polyester resins are elastic cracks. Use of classical formulae for elastic cracks has enabled estimates to be made of the time dependence of Young's modulus for both resins. Use of linear elastic fracture mechanics formulae has enabled stress intensity factors to be determined from measurements of crack profiles. Radial crack growth rates are small, in the range 10^{-12} ms^{-1} to 10^{-9} ms^{-1} for hot water tests, and remain constant over a wide range of stress intensity factor, from 0.3 to 0.8 $MPam^{1/2}$. Constant radial growth rate is compatible with a diffusion controlled mechanism, and analysis of the data indicates an activation energy of ~50 kcal. Some evidence is presented for concluding that, in polyesters only, the true nature of crack propagation is by way of slip/stick. The relevance of these findings to in-service interface lifetime prediction is discussed.

. Chemical reaction, adsorption and diffusion in polymers are all enhanced by stress and, as is the case for other materials, localised stresses, since they initiate failures, are more important than overall levels of residual stress. The solutions contained inside interfacial pressure pockets are corrosive and their destructive action, on the bonds responsible for load transfer, is enhanced by residual interfacial stress. There exist no high resolution techniques for measuring localised deformation in non-crystalline materials. In crystals, however, local *elastic* strain can be detected and measured using Kossel X-ray diffraction and electron beam back scattering diffraction in the SEM, and convergent beam diffraction in the TEM. Each of these facilities has been used to study residual stress close to α-quartz/epoxy resin interfaces in order to establish the general nature and magnitude of interfacial stress in SiO_2/epoxy composite materials including GRP. At 40nm from the interface the local strain is ~2%. The corresponding large interfacial stresses are held responsible for the observed very strong dependence of mechanical damping on interfacial area. - -

1. Introduction

Achievement of fibre reinforcement turns on the transfer of stress at fibre/matrix interfaces. The efficiency of interfacial load transfer decreases with time and, in polymer matrix composites, this decrease is attributed to the consequences of uptake of water from the in-service atmosphere. Diffused water accelerates mechanical degradation of interfacial bonds either directly or after dissolving or otherwise reacting with interfacial material to form corrosive solutions or reactants.

The work carried out during tenure of the present contract had two main thrusts, the first of which concerns the propagation of osmotic pressure filled resin cracks. Dissolution of solutes at the interface leads to the creation of interfacial pressure pockets which eventually propagate as cracks into the adjacent resin. Figure 12 in reference (1), shows examples of resin cracks at fibre interfaces (a) in E-glass/polyester resin and (b) in C-glass/polyester resin composites. Examples of resin cracks at fibre interfaces in a C-glass/polyester composite are shown in Figure 1. To fully understand loss of load transfer, it is evidently necessary to investigate the nature of osmotic pressure filled cracks in resin matrix materials. Such an investigation has been carried out for both epoxy and polyester systems. Of particular interest is the justification for using linear elastic fracture mechanics (LEFM) to describe accelerated test observations and to interpolate such descriptions to weathering in the field. With this in mind, it was necessary first to establish that cracks of the kind described in reference (1) are essentially elastic cracks, i.e. cracks which can be treated by LEFM.

The second main thrust concerns the accelerating effect on interfacial degradation of stress in addition to that arising from osmotic pressure generation. High resolution electron microscope techniques have been used to examine and measure the stress field at the interface in crystalline SiO_2/epoxy resin composites. By using α-quartz in place of glass it has been possible to make use of "state of the art" strain measurement methods afforded by Kossel X-ray diffraction, electron beam back scattering diffraction and convergent beam diffraction in order to detect and estimate strains in the SiO_2 at distances from the interface in the range 0-0.5 μm. The consequences anticipated for the effects on stress enhancement of interfacial reaction, adsorption and diffusion are discussed in the light of mechanical damping measurements on composites manufactured using fibres of different diameters, i.e. on composites characterised by different specific fibre/matrix interfacial areas.

2. Materials

Representatives of commercially available materials were used for the studies of osmotic pressure filled cracks. These were MY 750 epoxy resin supplied by Ciba-Geigy PLC and SR 18979 polyester resin supplied by BXL Plastics PLC. In the epoxy case, it was necessary to artificially add a solute (0.5 wt% of finely ground KCl) in order to promote internal cracking. The time required for loss of load transfer during water uptake is reported for composites manufactured from MY 750, MY 720, SP 250 epoxy resins; SR 18979 polyester resin; E glass, S glass, AS carbon, HU carbon commercial fibres; E glass, S glass laboratory drawn fibres. MY 750 epoxy resin, and natural quartz supplied by Gooch and Housego, were used to manufacture the electron microscope specimens on which very near interfacial deformations were measured.

SR 17449 polyester resin and fibres drawn from E-glass were used to fabricate specimens for the mechanical damping tests.

3.Equilibrium shape of an osmotic pressure filled crack

When formed, each interfacial pocket closely resembles a penny-shaped crack that has grown in a solid tensioned between fixed grips. The overall change in energy is from U_0, corresponding to the state of strain energy prior to fracture, to $U_0 - U_G$, where the Griffith energy U_G given by the Zener approximation is

$$U_G = \frac{1}{2} \frac{\sigma_1^2}{Y} \cdot \frac{4\pi\ ab^2}{3} = \frac{2\pi}{3} \sigma_1^2 \frac{ab^2}{Y} \tag{1}$$

$\sigma = \sigma_1$ is the tensile stress applied externally and perpendicular to the crack, Y is Young's modulus, a and b respectively are the half thickness and radius of the crack. Referring to Figure 2, if the interfacial cavity could be closed by application of traction on its wall, the stress σ_c acting across the cavity would rise from 0 to σ_1 and, correspondingly, its volume would decrease from V_1 to 0.

The Griffith energy gained by this process would be

$$U_G = \frac{1}{2} \sigma_1 V_1 = \frac{2\pi}{3} \cdot \frac{\sigma_1^2\ ab^2}{Y} \tag{2}$$

Hence

$$V_1 = 4\pi \cdot \sigma_1 \frac{ab^2}{3Y} \tag{3}$$

In reality, creation of the interfacial crack occurs with zero external stress. Its presence is due, instead, to creation of an internal pressure, and an internal pressure $p = \sigma_1$ gives the same V_1, see Figure 3.

$$V_1 = \frac{4\pi}{3} \cdot \frac{p \cdot ab^2}{Y} \tag{4}$$

and the elastic stored energy is

$$E_{el} = \frac{1}{2} p_1 V_1 = \frac{2\pi}{3} \cdot \frac{p_1^2\ ab^2}{Y} \tag{5}$$

Therefore
$$p_1 = \frac{3YV_1}{4\pi ab^2} \tag{6}$$

and
$$E_{el} = \frac{3Y}{8\pi} \cdot \frac{V_1^2}{ab^2} \tag{7}$$

A solute exerts an osmotic pressure[2] equal to the pressure that would be exerted by a gas having the same number of molecules in a volume equal to that occupied by the solution. Consider a change in volume of the interfacial cavity from V_0 to $V_0 + V_1$ resulting from dissolution of m moles of solute.

4

$$pV = mRT \tag{8}$$

The strain energy release $= \int p\,dV$

$$= \int \frac{mRT}{V}\,dV$$

$$= mRT \log_e \frac{(V_o + V_1)}{V_o}$$

$$= mRT \log_e \frac{p_1}{p_o} \tag{9}$$

p_o and p are the values of the osmotic pressure corresponding to volumes V_o and $V_o + V_1$ respectively.

The overall energy $E = E_{gas} + E_{elastic}$

$$= -mRT \log_e \frac{(V_o + V_1)}{V_o} + \frac{3}{8\pi} \frac{Y}{ab^2} V_1^2 \tag{10}$$

This function is sketched in Figure 4.

The value of V_1 corresponding to minimum energy release may be found by differentiation

$$\frac{dE}{dV_1} = -mRT \frac{1}{V_o + V_1} + \frac{3Y}{4\pi} \frac{V_1}{ab^2} \tag{11}$$

$$= 0 \text{ when } V_1^2 + V_1 V_o - \frac{4\pi}{3Y} ab^2 mRT = 0 \tag{12}$$

i.e. when

$$V_1 = \frac{-V_o}{2} \pm \sqrt{\frac{V_o^2}{4} + \frac{4\pi ab^2 mRT}{3Y}} \tag{13}$$

We must take the positive root, hence

$$V_1 = -\frac{V_o}{2} + \sqrt{\frac{4ab^2 mRT}{3Y} \left(1 + \frac{3YV_o^2}{16\pi ab^2 mRT}\right)} \tag{14}$$

$$\sim -\frac{V_o}{2} + \sqrt{\frac{4ab^2 mRT}{3Y}} \quad \text{for large values of b} \tag{15}$$

Alternatively, interfacial failure due to cracks inflated by osmotic pressure could be modelled as follows. Suppose a constant pressure reservoir supplies the "gas", then:

Energy, $E = -p_1 V_1 + \frac{1}{2}p_1 V_1 = -\frac{1}{2}p_1 V_1$

$$= -E_{elastic} = \frac{-2\pi}{3} \frac{p_1^2}{Y} ab^2 \tag{16}$$

but $E_{surface} \sim 2\gamma \pi ab$, where γ is the specific surface energy

so $E_{total} = 2\gamma \pi ab -\dfrac{2\pi}{3}\cdot\dfrac{p}{Y}_1{}^2 ab^2$ (17)

Differentiation of equation (17) with respect to b gives:

$$\frac{\partial E}{\partial b}total = 2\gamma\pi a - \frac{4\pi}{3}\cdot\frac{p}{Y}_1{}^2 ab$$

$$= 2\pi a\left(\gamma - \frac{2}{3}\frac{p_1{}^2}{Y} b\right) \qquad (18)$$

which is negative if

$$b > \frac{3Y\gamma}{2p_1{}^2} \qquad\text{ie if } p > \sqrt{\frac{3Y\gamma}{2b}} \qquad (19)$$

Differentiation with respect to a gives:

$$\frac{\partial E}{\partial a}total = 2\gamma\pi b - \frac{2\pi}{3}\frac{p_1^2}{Y} b^2 = 2\pi b\left(\gamma - \frac{p_1^2 b}{3Y}\right) \qquad (20)$$

and is negative if $b > \dfrac{3Y\gamma}{p^2}$ (21)

$\dfrac{\partial E}{\partial b}total$ is evidently more negative than $\dfrac{\partial E}{\partial a}total$, so the expression

for p_{crit} is taken from the former.

Taking as trial values $Y = 3GPa$, $\gamma = 1J/m^2$ and $b = 10\mu m$,

$$p_{crit} = \sqrt{\frac{3\times3\times10^9}{2}\frac{\times1}{10^{-5}}} = 10MPa \qquad (22)$$

Figure 5 shows the variation of osmotic pressure with solute concentration at 80C for aqueous solutions of three common inorganic solutes. The values for osmotic pressure were deduced from vapour pressure and compressibility data[3]. It is evident that relatively modest solute concentrations give rise to osmotic pressures in excess of the pressure required to stabilise the thin crack-like configuration of a pressure pocket.

However, water causes plasticisation of the resin, and so Y and γ will be reduced by a factor of, say, 10 each. The critical pressure for a 10μm crack would then be 1MPa, which is well within the osmotic pressures generated by dilute solutions.

4. Experimental study of osmotic pressure filled cracks

4.1 Elastic nature of resin cracks observed in accelerated tests

To demonstrate the elastic nature of osmotic pressure filled cracks in epoxy and polyester resins, and in particular to demonstrate the absence of any permanent (i.e. plastic) contribution to the crack opening displacement, a

6

number of cracks have been photographed and re-photographed after drying by annealing in air. This treatment causes the crack faces to come into contact with each other, Figures 6(a) and (b), and 7(a) and (b). Seen face-on, such cracks in dried samples generate interference patterns, Figure 8(a) and (b). By counting the fringes, the very close proximity of the crack faces can be measured, Figure 9. It could be argued that drying the resin might lead to the generation of negative pressure inside the crack. However, many of the cracks in dried resin are connected to the atmosphere by surface seeking cracks; a surface seeking crack is indicated by an arrow in Figure 8(b). In any case, creation of negative pressure would surely be relieved by the formation of bubbles containing occluded gas and/or low molecular weight material. The small residual space between the crack faces is attributed to obstruction by solute deposit after drying, see Figure 10.

4.2 Time dependence of Young's modulus

Elastic cracks, i.e. Griffith cracks, are elliptic in nature. This elliptic form has been re-examined by many authors including Sack[4], Sneddon[5], Elliott[6] and Westergaard[7]. The specific case of pressure-filled elastic cracks was considered by both Sack[4] and Sneddon[5]. Expansion of Westergaard's equation (4.6) gives

$$\eta^2_o = \frac{-4(1-v^2)^2 \, p^2 \, x^2}{E^2} + \frac{4(1-v^2)^2 \, p^2 \, a^2}{E^2} \qquad (23)$$

where η_o = half crack opening displacement
x = distance measured from the crack centre
a = length of semi-minor axis of the crack
v = Poisson's ratio
E = Young's modulus

When formed, osmotic pressure filled cracks often contain resolvable undissolved solute. Undissolved solute can be seen at the centre of the crack shown in Figure 10 for example. The water solution within such cracks is evidently saturated with solute. The osmotic pressure, estimated in reference (8) for the saturated hot water solution identified in cracks inside the polyester resin system designated system A in that reference, is 473.3 bars. Some of the present accelerated test data were obtained using the same resin in water immersion tests at 70, 80 and 94C. Since osmotic pressures for saturated solutions of common inorganic solutes increase only marginally in this temperature range, a constant value of 500 bars was assumed when using equation (23) to compute the respective magnitudes of E from data such as that shown in Figure 11. Static values for E were determined on the same samples by simultaneous measurements of the longitudinal and transverse sound wave velocities at 5Mhz; no significant differences from the room temperature value of 4.0 GPa for the dry resin were found. It is therefore concluded that the variations in E obtained from Figure 11 are attributable solely to its time dependence. Figure 12 summarises the data.

4.3 Measurement of crack growth rates

Figure 13(a) and (b) shows edge on views of a penny-shaped crack in epoxy and polyester resin samples photographed after several times of immersion in water at 94C. Measurements of the crack diameter reveal that the radial crack growth

rates are constant at $4.9 \times 10^{-10} \text{ms}^{-1}$ and 1.1×10^{-9} ms^{-1} respectively. The same experiment on cracks in polyester specimens immersed in water at 70C and 80C reveal constant crack growth rates of 5×10^{-12} ms^{-1} and 7×10^{-11} ms^{-1} respectively.

The following argument demonstrates that constant radial growth rate, at a given temperature, is dimensionally compatible with a diffusion controlled mechanism for fracture.

The total flux of water entering the crack is

$$J \propto \frac{d}{dt}(V) \tag{24}$$

where V is its volume

If Young's modulus (E) is constant then putting x=0 into equation (23) we see that, at the centre of the crack, the crack opening displacement is proportional to the crack radius (a). Hence $V \propto a^3$ and $J \propto a^2 da/dt$ which, since da/dt is found experimentally to be constant, implies that J is proportional to a^2.

If the fracture process is diffusion controlled then, by Fick's first law, the flux across unit area is

$$j = -D \frac{\partial c}{\partial x} \tag{25}$$

where the diffusion coefficient (D) is a constant. The concentration gradient $\partial c/\partial x$ is also constant since, with undissolved solute always present (refer to Section 4.2), the concentration of water in the electrolyte, as well as that in the environment outside the specimen, is constant. The catchment area across which water entering the crack must diffuse, i.e. the surface area of the crack, is proportional to a^2. Hence for a diffusion controlled mechanism we expect J = j x catchment area to be proportional to a^2.

The activation energy (Q) for this mechanism may be estimated from the rate as follows

$$\text{rate} \propto e^{-Q/kT} \tag{26}$$

$$\log_e(\text{rate}) = \frac{-Q}{kT}$$

$$\frac{d(\log_e(\text{rate}))}{dT} = \frac{Q}{kT^2}$$

$$Q = kT^2 \frac{d(\log_e(\text{rate}))}{dT} \tag{27}$$

For polyester resin, the rate of radial crack growth increases by one order of magnitude between 70 and 80C

8

Hence
$$Q = 2(350)^2 \frac{\times 2.3}{10} \text{ cals}$$

$$= 0.5 \times 10^5 \text{ cals}$$

$$= 50 \text{ kcals}$$

this is a somewhat high value for the activation energy for diffusion of water in resins.

The assumption that Young's modulus (E) is constant is not valid. Using equation (23) the crack volume $V \propto (a/E)^3$ which since E increases with volume gives $V \propto a^{<3}$. Experimentally we find $V \propto a^{2.6}$ for both resins from which it is concluded that water diffusion alone is not rate determining.

4.4 Crack surface topography

In the case of polyester samples close inspection of the crack surfaces has sometimes revealed the presence of more or less concentric steps, i.e. abrupt changes in fracture path. Examples can be seen on the crack surface shown in Figure 14. The steps delineate positions at which the crack was presumably at rest and are assumed to be direct evidence for a slip/stick mode of crack propagation.

Crazing is the precursor to fracture in many polymeric materials, the occurrence of which immediately suggests a model for slip/stick crack propagation. The craze is comprised of highly drawn material and, since the necking down phenomenon which gives rise to high draw ratio is a characteristic of high temperature drawing, it is evident that a zone of high temperature material must exist ahead of the craze. For polymers, room temperature is near the melting temperature so high temperature probably means just a few degrees above room temperature. Intermittent falls in temperature, and hence interruptions of the necking down process associated with crazing, would be expected to cause crack arrests until the stress is raised sufficiently to reheat the craze leader. The small changes in fracture path each time crack growth resumes is in accordance with Griffith's[9] evaluation of the tensile stress at the surface of and tangential to an elliptic cavity in a plate subjected to principal stresses σ_1 and σ_2, respectively making angles Φ and $\pi/2 - \Phi$ with the major axis of the ellipse. Inglis[10] considered the case of an elliptic hole in a plate subject to a tensile stress σ applied in a direction making an angle Φ with the major axis of the ellipse, Figure 15(a), and found that the tensile stress at the surface of and tangential to the hole is

$$\sigma_{\beta\beta} = \sigma \left\{ \frac{\sinh 2\alpha_0 + \cos 2\Phi - e^{2\alpha_0}\cos 2(\Phi - \beta)}{\cosh 2\alpha_0 - \cos 2\beta} \right\} \tag{28}$$

Referring to Figure 15(b) for $\sigma_2 = 0$ the Inglis solution, with the sense of increasing β reversed gives

$$\sigma_{\beta\beta} = \sigma_2 \left\{ \frac{\sinh 2\alpha_0 + \cos 2\Phi - e^{2\alpha_0}\cos 2(\Phi - \beta)}{\cosh 2\alpha_0 - \cos 2\beta} \right\} \tag{29}$$

and for $\sigma_1 = 0$ it gives

$$\sigma_{\beta\beta} = \sigma_1 \left\{ \frac{\sinh 2\alpha_o + \cos 2(\pi/2 - \Phi) - e^{2\alpha_o} \cos 2(\pi/2 - \Phi + \beta)}{\cosh 2\alpha_o - \cos 2(-\beta)} \right\} \qquad (30)$$

Hence by superposition,

$$\sigma_{\beta\beta} = \frac{(\sigma_1 + \sigma_2) \sinh 2\alpha_o + (\sigma_1 - \sigma_2) \left\{ e^{2\alpha_o} \cos 2(\Phi - \beta) - \cos 2\Phi \right\}}{\cosh 2\alpha_o - \cos 2\beta} \qquad (31)$$

The values of Φ and β for which $\sigma_{\beta\beta}$ is a maximum are found by differentiation. Putting $\partial \sigma_{\beta\beta}/\partial \beta = 0$ and taking as solution $\sin 2\beta = A\alpha_o + O(\alpha_o^2)$, it can be demonstrated that $\sigma_{\beta\beta}$ is a maximum at *two pairs of points* on each crack. If $\Phi = 0$ or $\pi/2$, these points are at the ends of the major and minor axes respectively. For all other values of Φ both pairs of points are very near the ends of the major axis as sketched schematically in Figure 16(a). The two extremal values of $\sigma_{\beta\beta}$ always have opposite sign. Continuation of fracture from one such point, thereby leaving a step on the fracture surface, is illustrated in Figure 16(b).

The classical crazing material is polystyrene. The fact that the polyester resin studied here contains styrene as monomer may explain the evidence of slip/stick fracture shown in Figure 14. No such evidence was seen on the faces of cracks in epoxy samples.

5. Application of fracture mechanics to osmotic pressure filled cracks

Fracture mechanics is concerned with the propagation of atomically sharp cracks. It may well be that, when propagating, osmotic pressure filled cracks in polyester resin are indeed atomically sharp. It may also be the case that the periods of propagation are short in which case the time dependence of elastic modulus may be ignored and *linear* elastic fracture mechanics (LEFM) may be used to describe the cracks. In the following analysis, both these assumptions are made.

5.1 Crack growth times

The usual starting point for analysis of crack growth in inorganic glasses[11] is the parabolic relationship between stress intensity factor (K) and crack length (a)

$$K = \sigma \, Y \sqrt{a} \qquad (32)$$

σ is the tensile stress normal to the crack and Y is a constant determined by the crack geometry.

In resin matrix composite materials, cracks can nucleate and grow in the absence of any externally applied stress; the driving force for fracture is derived from osmosis[1,8] with each crack containing an internal osmotic pressure (p). The Griffith energy (U_G), the elastic free energy released on creation of a penny-shaped crack inflated by an internal pressure (p), is identical to that for a crack of the same lateral dimensions formed in the presence[5] of a previously uniform uniaxial stress $\sigma = p$ applied normal to its plane

$$U_G = \frac{8(1 - \nu^2) \, a^3 \, p^2}{3E} = \frac{1}{2} pV \qquad (33)$$

v is Poisson's ratio, E is Young's modulus and V is the elastic expansion, i.e. the volume, of the crack. Hence it is concluded that p may be substituted for σ in equation (32) in order to obtain an equation for the stress intensity factor for a pressure filled crack

$$K = p Y \sqrt{a} \tag{34}$$

where the constant Y is of order unity

Using van't Hoff's[2] formula for the osmotic pressure (p) of a dilute solution, equation (8), and assuming that m, the number of moles of dissolved solute, remains unchanged during crack growth, substitution of V from equation (33) gives

$$p = ka^{-3/2} \tag{35}$$

where the constant k is given by $k^2 = \dfrac{3mRTE}{16(1 - v^2)}$ $\tag{36}$

Values of k^2 for each of four individual cracks have been calculated assuming a solute content of 10^{-10} mole, and are reported in Table 1.

Hence, equation (34) becomes $\qquad K = \dfrac{Yk}{a}$ $\tag{37}$

It should be noted that, whereas for crack growth in a monolithic solid subjected to an applied stress which does not vary with time, K increases with crack growth (equation (32)), the case for pressure filled cracks concerns a K which decreases with crack growth (equation (37)).

Re-arranging equation (37) and differentiating we get

$$v = \frac{da}{dt} = f(K) = -\frac{Yk}{K^2} \cdot \frac{dK}{dt} \tag{38}$$

Hence the time required for a crack inflated by osmotic pressure to propagate under the action of that pressure is

$$t = -Yk \int_{K_{I\ initial}}^{K_{I\ final}} \frac{dK}{K^2 v}$$

$$= \frac{Yk}{v} \left[\frac{1}{K_{I\ final}} - \frac{1}{K_{I\ initial}} \right] \quad \text{if } v \text{ is constant} \tag{39}$$

In the present case, since p is constant equation (34) and not equation (37) must be used for K. Hence the time for crack propagation is

$$t = \frac{2}{p^2 Y^2 v} \int_{K_{I\ initial}}^{K_{I\ final}} K\ dK$$

$$= \frac{1}{p^2 Y^2 v} \left[K^2_{I\ final} - K^2_{I\ initial} \right] \quad \text{if } v \text{ is constant} \tag{40}$$

11

Table 1   Values of $k^2 = \dfrac{3mRTE}{16(1-v^2)}$ for osmotic pressure filled cracks

Resin	Temperature T(K)	Young's Modulus $E(GNm^{-2})$	k $(Nm^{-1/2})$
epoxy	367	0.37 − 0.72	4.06 − 5.70
polyester	343	0.55 − 0.59	4.82 − 5.00
	353	0.35 − 0.56	3.90 − 4.93
	367	0.86 − 1.22	6.23 − 7.42

5.2 Stress intensity factors

The cracks described here are elastic cracks and, if they can be described by linear elastic fracture mechanics, measurements of their profiles can be used to obtain values for stress intensity factor (K_I). Eshelby's[12] equation (2.10) for the parabolic relationship between crack opening displacement (ΔV) and distance from the crack tip (r) is

$$\Delta V = \frac{K_I}{(2\pi)^{1/2}} \cdot r^{1/2} \cdot \frac{8(1-v^2)}{E} \qquad (41)$$

Figure 17 shows plots of ΔV versus $r^{1/2}$ for cracks at 94C, from the slopes of which, stress intensity factors have been calculated. These and the corresponding crack velocities are presented in the form of V-K relationships in Figure 18. For a given immersion water temperature, the velocity remains constant even when, due to changes in pressure, the stress intensity factor varies.

Figure 18 contains sufficient data to check the validity of equation (40). Taking just two of the cracks, namely the epoxy at 94C and the polyester at 94C, the maximum predicted times of propagation are for the epoxy:

$t = 4.3 \times 10^5$ seconds compared with 2.56×10^5 seconds actual

and for the polyester:

$t = 1.65 \times 10^5$ seconds compared with 1.88×10^5 seconds actual

The agreement is good and lends credence to the approach adopted.

Osmosis at fibre/matrix interfaces causes loss of interfacial load transfer, the development of which has been monitored for several composite systems by studying and measuring changes in the optical anisotropy, arising from the net shrinkage of resin on to short fibres, that remains after curing. Data for a variety of composite systems were reported in DAERO-78-G-117 Annual Technical Report, Oct. 78-Oct. 80 and in DAJA-37-81-C-0214 Annual Technical Report, Apr. 81-Mar.82. Table 2 summarises this data. Experimental observation reveals that, whenever cracks nucleated at the fibre/resin interface are clearly resolved, their paths are located wholly within the matrix material, i.e. the onset of increased compliance commensurate with loss of load transfer ability is attributable to creation of resin cracks adjacent to the interface. For a

Water Temperature (C)	Resin	Fibre	Time for loss of load transfer
100	MY 750	commercial E-glass	18 hours
"	"	E-glass drawn in carbon tetraflouride	16 minutes
"	"	E-glass drawn in ammonia	< 1 hour 30 mins
"	"	"	~ 1 hour 45 mins
"	"	S-glass drawn in ammonia	22 hours
"	"	"	22 hours
"	"	commercial AS carbon	~ 9 hours
"	"	commercial HU carbon	~ 15 minutes
"	SR 18979	commercial E-glass	4 minutes
"	"	"	4 minutes 45 secs
"	"	untreated E-glass	6 minutes
"	"	"	11 mins 10 secs
80	MY 750	commercial S-glass	51 days 6 hours
"	"	"	> 50 days
"	MY 720	commercial E-glass	< 2 hours
"	"	commercial S2-glass	< 2 hours
"	"	"	1 hour
"	"	commercial S1-glass	< 4 days
"	"	S-glass drawn in ammonia	~ 20 hours
"	SP 250	commercial S2-glass	< 5 days
60	MY 750	commercial E-glass	> 10 days
"	"	"	> 10 days
"	"	E-glass drawn in carbon tetraflouride	> 10 days
"	"	"	> 10 days
"	"	commercial S-glass	> 10 days
"	"	"	> 10 days
"	"	S-glass drawn in ammonia	5 hours 35 mins
"	"	"	5 hours 12 mins
ambient	"	E-glass drawn in ammonia	40 - 53 days
"	"	"	40 - 53 days
"	"	S-glass drawn in ammonia	36 - 49 days
"	"	"	36 - 49 days
"	"	commercial AS carbon	> 81 days
"	"	commercial HU carbon	> 81 days
"	MY 720	commercial E-glass	> 8 days
"	"	commercial S1-glass	> 8 days
"	"	commercial S2-glass	8 days
"	"	"	8 days
"	"	E-glass drawn in ammonia	9 days
"	"	S-glass drawn in ammonia	9 days
"	SP 250	commercial S2-glass	25 days
"	SR 18979	commercial E-glass	18 hours 12 mins

Table 2. Time taken to lose load transfer during exposure to water of various composite materials (refer to DAERO-78-G-117 Annual Technical Report, Oct 78-Oct 80: DAJA-37-81-C-0214 Annual Technical Report, Apr 81 - Mar 82

13

given resin and water exposure temperature, the crack velocity and hence the time for crack growth can be obtained from plots of the kind shown in Figure 18. The difference between this time and the time for loss of load transfer is the time taken for diffused water to initiate interfacial degradation.

Taking as example E glass fibre composites, the solute responsible for interfacial pressure pockets is the 0.6% by weight of modifying oxides in the glass[1]. Etch pits representing the individual volumes of material leached from E glass fibres measure at most a micron across, see Figure 19. If each such volume gives rise to a crack, it corresponds to $\sim 10^{-14}$ moles $Na_2O + K_2O$. Hence, at 100C, k^2 in equation (36) is of order $145N^2m^{-1}$ for the MY 750 epoxy composites, in Table 2. Taking as trial values, $Y = 1$, $k = 12$ $Nm^{-1/2}$, K_I final $= 0.30$ $MPam^{1/2}$ and K_I initial $= 0.79$ $MPam^{1/2}$, equation (39) gives $t = 11$ hours 42 minutes for the expected time of crack growth. This is less by some 6 hours than the time required for total loss of load transfer, i.e. crack growth was initiated after ~ 6 hours of water uptake.

When aided by sources of internal stress other than osmosis, or by application of external stress, the crack propagation behaviour can be expected to move to V-K relationships for higher temperatures (see Figure 18). This is to be expected because of the role of stress in terminating and therefore shortening the periods or crack arrest during slip/stick crack propagation (see section 4.4). When enthalpy data for crazes become available, it will be possible to anticipate the inter V-K transitions for different superimposed stresses, i.e. it will be possible to use Figures like Figure 18 for design purposes.

6. Fibre/matrix interfacial stress

Models for fibre reinforcement, e.g. that proposed by Cox[12], assume that there is no radial distribution of axial fibre stress. The same models predict a dependence of mechanical properties on fibre volume that is independent of fibre diameter and therefore independent of specific interfacial area (fibre/matrix interfacial area per unit volume of composite). Since both the assumption and the prediction have a bearing on the state of stress at the interface and hence on the enhancement by stress of interfacial chemical reaction, adsorption and diffusion, experiments have been devised whereby both can be studied.

7. Radial distribution of axial fibre stress

There are no direct experimental methods for detecting and measuring local strain close to the glass fibre/epoxy resin interface. However, to a first approximation, the chemical bonding and hence the efficiency of load transfer between the two materials is not expected to depend on the physical nature of the SiO_2 used as fibre material and, since there are available a number of high resolution electron optical techniques for detecting and measuring local deformations in crystalline materials, experiments have been carried out on α-quartz/epoxy resin composites.

In order to use electron microscopes to measure local strain levels three approaches were considered: Kossel X-ray diffraction (KXD) and electron back scattering diffraction (EBSD) in the scanning microscope, and convergent beam diffraction (CBD) in the transmission electron microscope (TEM). These methods are based on the diffraction of x-rays or electrons by α-quartz crystal lattice planes according to Bragg's law ($2d \sin \theta = n\lambda$). Any change

in lattice parameters, as a result of elastic strain, causes a corresponding change in the observed diffraction pattern. Experiments were designed with the particular aim of applying the methods to strain measurements near the interfaces of α-quartz/epoxy resin composite materials. There are three important factors to be considered when applying these techniques to such measurements: (a) spatial resolution (i.e. the volume from which the strain is measured), (b) the accuracy (related to sensitivity) of the strain measurement, and (c) the time and difficulties involved in preparing suitable specimens.

Two kinds of bulk specimen were fabricated, each consisting of a concentric cylinder of one material inside the other. The first manufacturing operation was core drilling of the quartz single crystal, the technique of which has been previously reported[14]. Resin was cast around the α-quartz core when making one kind of specimen, and inside the α-quartz tube when making the other kind. Before casting, the quartz surfaces were thoroughly cleaned first chemically, and then by ion beam etching. After curing the resin, a diamond saw was used to slice specimens suitable for electron microscopy. The TEM slices were mechanically ground to ~ 100 μm thickness and further thinned by ion beam etching. The SEM slices were mechanically ground and etched in fused caustic soda and/or HF solution in order to remove any mechanical deformation introduced by grinding. Since both component materials are insulators, the specimens had to be coated with a thin conducting layer of amorphous carbon in order to prevent charging in the electron beam.

The instruments used for the present studies were a Cambridge Stereoscan S4 scanning microscope and a Philips EM400 transmission microscope. The accuracies and resolutions quoted below are for these particular instruments.

7.1 EBSD

In this technique the inelastically backscattered and diffracted primary electrons can be used to observe and determine changes in lattice parameters. The escape depth of these electrons is typically 10 nm so the diffraction information obtained is from a very small volume at the specimen surface. To a good approximation the spatial resolution is determined by the area illuminated by the incident beam and is typically of 1 μm diameter. The accuracy (and sensitivity) of strain measurement is mainly limited by the energy spread in the electron beam and is typically 1 in 500. Owing to the small escape depth of the electrons, the conducting layer may adversely contribute to the observed diffraction pattern; the layer can be expected to rescatter and partially absorb the backscattered electrons thereby making the diffraction pattern diffuse and low in contrast (low signal to noise ratio).

Figure 20(a) and (b) shows examples of contrast enhanced print-negatives of EBSD patterns from α-quartz. Such diffraction patterns were recorded at various distances from the resin interface, ranging from within 3 μm up to 1 mm, and with the α-quartz in various crystallographic orientations. Approaching the α-quartz resin interface there is no observable change in the EBSD pattern until the distance of approach is 5 μm or less. Within this distance the diffraction lines are increasingly diffuse due to local straining and indicate strain levels of up to 2%. This diffraction pattern contrast is typical of strains in excess of the elastic limit.

7.2 CBD

Variations in lattice parameters can also be measured by observing the shift in position of high order Laue zone (HOLZ) lines in a CBD pattern. The spatial resolution of a few 10 nm is far superior to that of KXD and EBSD. The typical accuracy of 1 in 5000 is also considerably better than that of EBSD. The main disadvantage of the CBD technique concern difficulties in preparing suitable TEM foils. Conventional etching techniques were found to produce preferential etching of one or other phase, giving an electron transparent region of that phase well away from the interface.

CBD patterns have been recorded at distances varying from 15 μm down to 800 nm from the quartz-epoxy interface. Figure 21(a), (b) and (c) shows examples of such patterns. In the region from 4 μm to 15 μm from the interface there is no observable strain in the quartz. With the type of pattern shown strain levels of 0.05% can be detected. At 3.5 μm from the interface, changes in position of HOLZ lines and Kikuchi lines are observed. Figures 21(a) and (b) demonstrate this change for positioning of the electron probe at distances from the interface of 3 μm and 1.3 μm respectively. The HOLZ lines move in unison with respect to the central disc without moving relative to each other. This is attributed to strain relief through specimen buckling, i.e. no residual lattice strain remains. At distances as close to the interface as 800 nm, buckling is still observed, but closer than this there is a sudden drastic deterioration in sharpness of the HOLZ lines, Figure 21(c). This is indicative of a high rate of change of lattice strain. The estimated amount of buckling as a function of distance from the interface is plotted in Figure 22.

The CBD observations are in agreement with those of EBSD in that the interfacial strain of the α-quartz is localised and approaches zero at 5 μm from the interface.

7.3 KXD

This is the most accurate of the techniques considered. Changes in lattice parameter as small as 1 in 10^4 can be detected. The spatial resolution, however, is inferior to that for EBSD and CBD. Spatial resolution is determined by the electron-specimen interaction volume which is pear-shaped and of the order of $10 \times 10 \times 10$ μm^3. If the wavelength of the characteristic X-rays produced within this volume is such that

$$\frac{2d}{n\lambda} = \sin \theta > 1 \tag{42}$$

then the pseudo-Kossel technique has to be applied. This is the case with α-quartz. In pseudo-KXD a fine-grain powder (e.g. Cu) is sprinkled onto the specimen surface and X-rays produced in a single grain so that $\lambda > 2d/n$. Apart from that the specimen preparation is relatively simple. Practical problems do arise, however, with crystals that have a high degree of perfection because the diffraction lines then become too sharp to be easily detected. Although imperfections reduce the line intensity, they also broaden the lines.

Several unsuccessful attempts were made at recording Kossel-patterns from α-quartz/epoxy resin specimens. The signal to background ratio was optimized by preparing a thin wafer and allowing the X-rays to propagate through the

specimen to a depth for which $1.5 < \mu t < 2.5$. (μ = linear absorption coefficient). This attempt failed to produce an observable KXD pattern.

7.4 Discussion

Figure 23 shows an SiO_2^{4-} tetrahedron model of α-quartz and reveals open channels as a prominent feature. The model is viewed along the crystallographic a-direction and two kinds of channel are evident; the hexagonal channel is lined with a double helix of corner sharing tetrahedra and the rectangular channel is lined with a single helix of corner sharing tetrahedra. There exists plenty of room for penetration by liquid resin. Such penetration, which may well be aided by coupling agents, is the origin of interdigitation between the two solid phases, i.e. between the α-quartz and the cured resin.

Differential contraction between the two phases takes place during cooling from the cure temperature and renders the interdigitated regions self-stressed. Interdigitation, rather than strong bonding at the interface, is believed to be the principal source of interfacial strain.

To better simulate glassy SiO_2, dislocated α-quartz was used, see Figure 24. The Burgers vectors are parallel to the helix channels and convert double helices into either single or triple helices, and single helices into either rings or double helices. The quartz also contains defects in the form of Dauphiné twin boundaries. It is evident, therefore, that the best possible approximation to a glass/resin interface has been achieved in these experiments.

8. Energy dissipation at fibre/resin interfaces during fatigue deformation

In order to demonstrate that the fibre/matrix interface is an important location for dissipation of energy during mechanical deformation, vibratory tests have been carried out by D Short[14] on a series of glass/epoxy composites, each member of the series having fibres of a different diameter in the range 20-70 μm. The test pieces were fabricted with rectangular cross-section and vibrated transversely in the first free-free mode. The specimen supports are moveable so that they can be positioned at the nodes. Excitation is by a coil attached to the mid-point of the test-piece. The coil sits in the field of a permanent magnet and is energised so that vibration with constant amplitude at the resonant frequency is maintained.

Figure 25 summarises the data obtained from these tests. The specific damping capacity is defined as the ratio of the energy dissipated per cycle to the maximum energy of the system. The data clearly shows that at any fibre volume fraction, more energy per cycle is dissipated in small than in large fibre diameter specimens, i.e. in large rather than small interfacial area specimens.

A pilot experiment, using fibres coated with thermographic paints supplied by Raychem Corporation, did not reveal any resolvable indications of interfacial temperature changes during cyclic loading. The heating time (t) for a fibre of radius r is

$$t = \frac{r^2}{\alpha} \qquad (43)$$

where the thermal diffusivity is

$$\alpha = \frac{\kappa}{\rho c} \tag{44}$$

κ is the thermal conductivity, ρ is the density and c the specific heat capacity of the fibre material. Substituting for fibreglass $r_o = 5\mu m$, $\kappa = 0.85$ $Wm^{-1}K^{-1}$, $\rho = 2.5$ gcm^{-3} and $c = 0.5$ $Jg^{-1}K^{-1}$ we get $\alpha = 6.8 \times 10^{-3}$ $cm^2 s^{-1}$ and $t \sim$ $1\mu s$. Hence it is concluded that temperature gradients originating at the interface are unlikely to be measured during a half cycle at 100Hz.

In the absence of any direct evidence for the identity of mechanisms by which interfacial energy is generated during fatigue cycling, it is possible only to speculate. Friction due to differential axial displacement across debonded interfaces is a likely candidate. However, osmotic pressure filled interfacial cracks do not easliy lend themselves to such a mechanism. It is therefore instructive to repeat the above experiments in a humid atmosphere. Preliminary such experiments appear to contradict the simpleminded expectation and this in turn leads us to invoke the overiding importance of the residual interfacial stresses reported in Section 7. The larger the specific interfacial area, the larger the overall contribution to interfacial damage by stress corrosion attributable to residual interfacial stress.

9. Publications

"Measurement of the stress field created within the resin between fibres in a composite material during cooling from the cure temperature"
B Cunningham, J P Sargent, K H G Ashbee
J Mater Sci (1981) 16, 620-626

"On the occurrence of osmosis during water uptake by adhesively bonded joints"
J P Sargent and K H G Ashbee
J Phys D (1981) 14, 1933-1938

"Adhesive joints involving composites and laminates. Measurement of stresses caused by resin swelling"
J P Sargent and K H G Ashbee
J Composite Materials (1981) 15, 492-501

"Internal stresses in fibre reinforced plastics"
K H G Ashbee, J P Sargent and Elizabeth Walter
Proc NSF-CNR Symposium on Composite Materials, Capri, June 15-19 1981, ed. J C Seferis and L Nicolais, published by the Plenum Publishing Company Limited (1982)

"Measurement of swelling stresses by optical interferometry"
J P Sargent and K H G Ashbee
Proc 19th Annual conference on Adhesion and Adhesives, London,
March 31-April 1 1981, ed. K W Allen, published by Applied Science Publishers (1982) 135-148

"The irreversibility of dimensional changes in epoxy adhesives undergoing uptake and expulsion of water"
J P Sargent and K H G Ashbee
Polymer (1982) 23, 327-331

"The deformation of the adherends in an adhesive joint undergoing water uptake"
D E Jesson and J P Sargent
J Adhesion (1982) 14, 119-128

"Direct comparison of loss of load transfer to "E" and "S" glass fibres manufactured by drawing into different environments"
M Vaudin and K H G Ashbee
J Mater Sci (1982) 17, 1329-1336

"On the assumption that epoxy-based adhesives are free from shear stress during cure"
J P Sargent and K H G Ashbee
I@EC Product Research and Development (1982) 21, 302-304

"Osmosis in composite materials"
Elizabeth Walter and K H G Ashbee
Composites (1982) 13 365-368

"Glass reinforced plastics as optical waveguides - a method for NDE of GRP"
N R Farrar and K H G Ashbee
NDT International (1983) 16 13-15

"Pressure filled interfacial cracks"
K H G Ashbee
Polymer Preprints (1983) 24 187-188

"Osmotic pressure filled cracks"
J P Sargent and K H G Ashbee
In "Composites, Interfaces" editor B M Culbertson, ACS Symposium Series No (1983)

"Osmosis a failure mechanism in fibre reinforced composites"
Elizabeth Walter and K H G Ashbee
Canadian Metallurgical Quarterly (1983) in press

"The dimensional Stability of Epoxy Adhesive Joints"
J P Sargent
In "Adhesive Joints: Formation, Characteristics, and Testing." K L Mittal, Editor, Plenum Press (1983) in press

References

(1) K H G Ashbee and R C Wyatt, Proc Roy Soc (1969) A312 553

(2) J van't Hoff, Phil. Mag. (1888) 26:81 2662

(3) Landolt-Bornstein 'Physikalisch-Chemische Tabellen', (Springer-Verlag, Berlin, 1936) p2663

(4) R A Sack, Proc Phys Soc (1946) 58 729

(5) I N Sneddon, Proc Roy Soc (1946) A187 229

(6) H A Elliott, Proc Phys Soc (1947) 59 208

(7) H M Westergaard, J Appl Mech (1939) A49

(8) K H G Ashbee, F C Frank and R C Wyatt, Proc Roy Soc (1967) A300 415

(9) A A Griffith, 1st Intl. Conf. Appl. Mech. (Delft 1924) 55

(10) C E Inglis, Trans. Inst. Naval Architects (1913) 55 219

(11) A G Evans, J. Mater. Sci. (1972) 7 1137

(12) J D Eshelby, Sci Prog, Oxf (1971) 59 161

(13) H L Cox, Brit. J. Appl. Phys. (1952) 3 72

(14) T W Turner and K H G Ashbee, Final Tech. Rept. US Army Grant DA-ERO-76-G-068 (1978)

(15) D Short, MSc Thesis, University of Bristol (1969)

Figure captions

Figure 1   Resin cracks accompanying loss of load transfer in a C-glass/polyester composite, C-glass contains 9.6 wt% Na_2O. Specimen immersed in boiling water for 20 hrs.
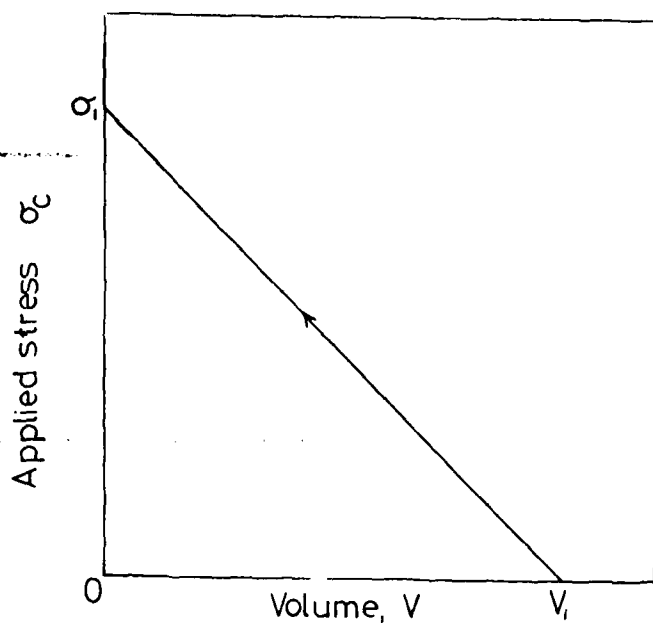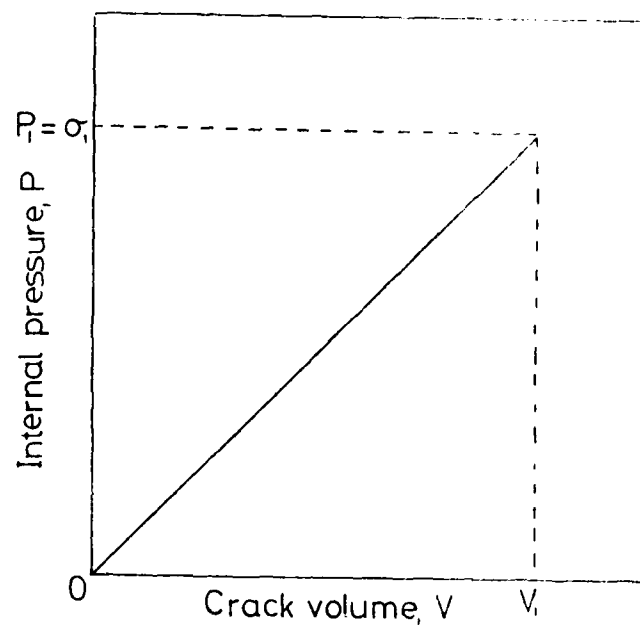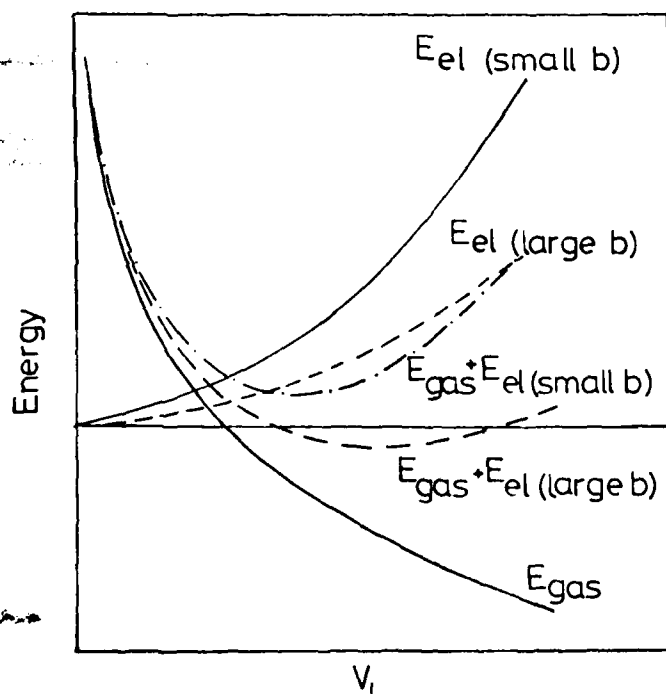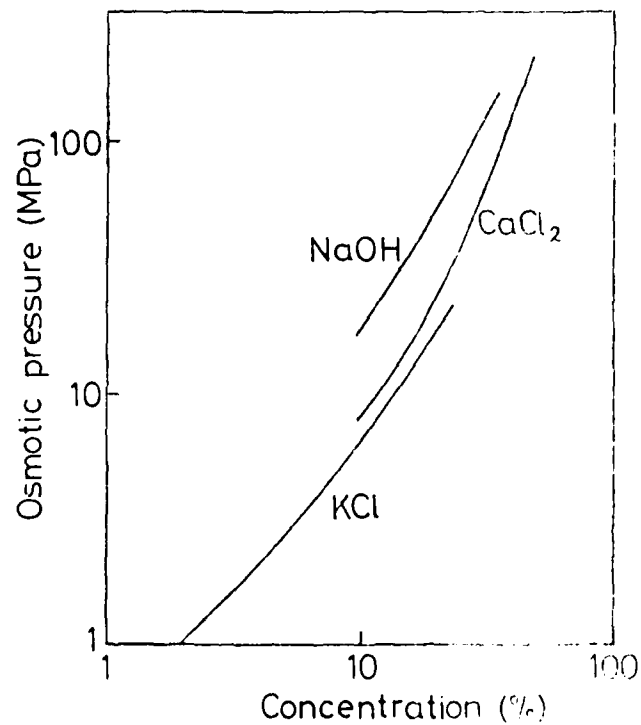
Figure 2   Applied stress as a function of volume of a Griffith's crack

Figure 3   Crack volume vs internal pressure for an inflated crack

Figure 4   Energy vs volume of an inflated crack

Figure 5   Osmotic pressure vs solute concentration for some common inorganic solutes
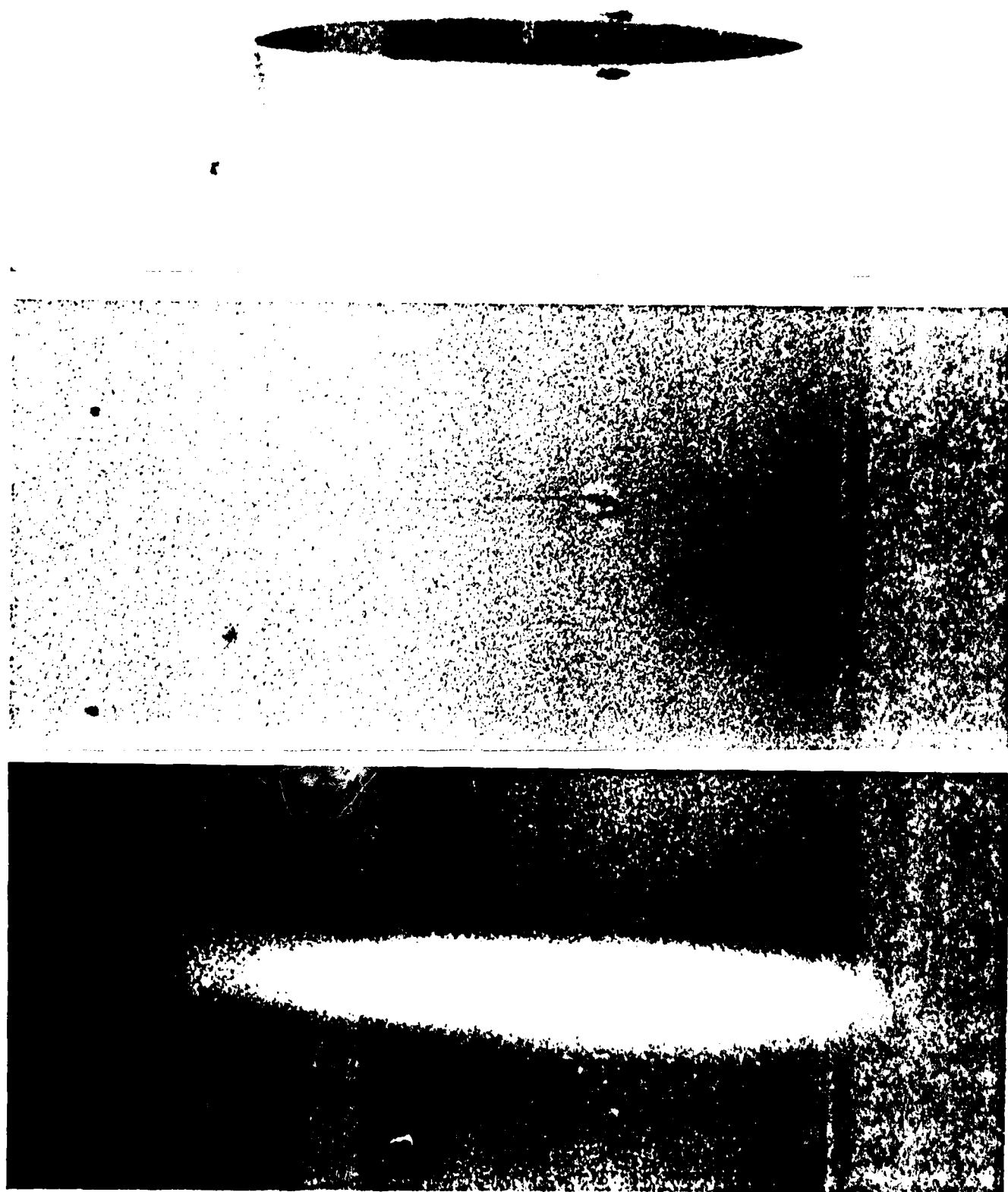
Figure 6(a)   Penny-shaped crack in KCl-doped epoxy resin photographed edge-on. 140 hrs immmersion in water at 94C

(b)   Same crack after drying in air for 1 hr at 100C

(c)   Same as (b) with polarisers crossed. The flare of bright contrast is attributed partly to change of polarisation of light reflected by the crack faces and, more importantly, to permanent molecular orientation in resin immediately adjacent to the crack.
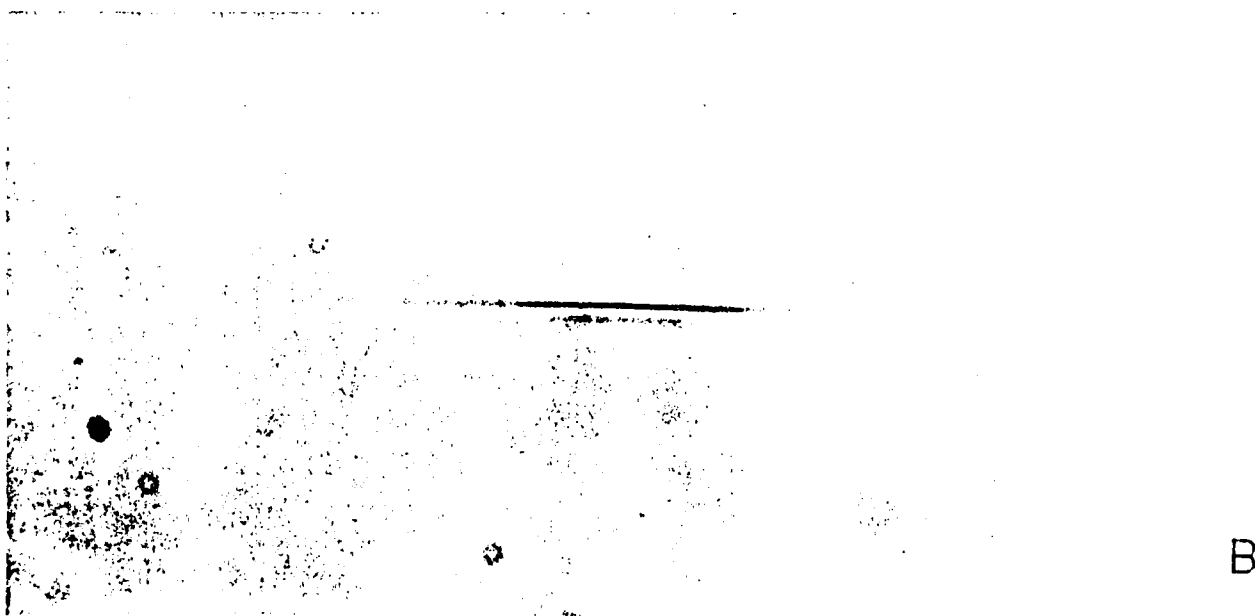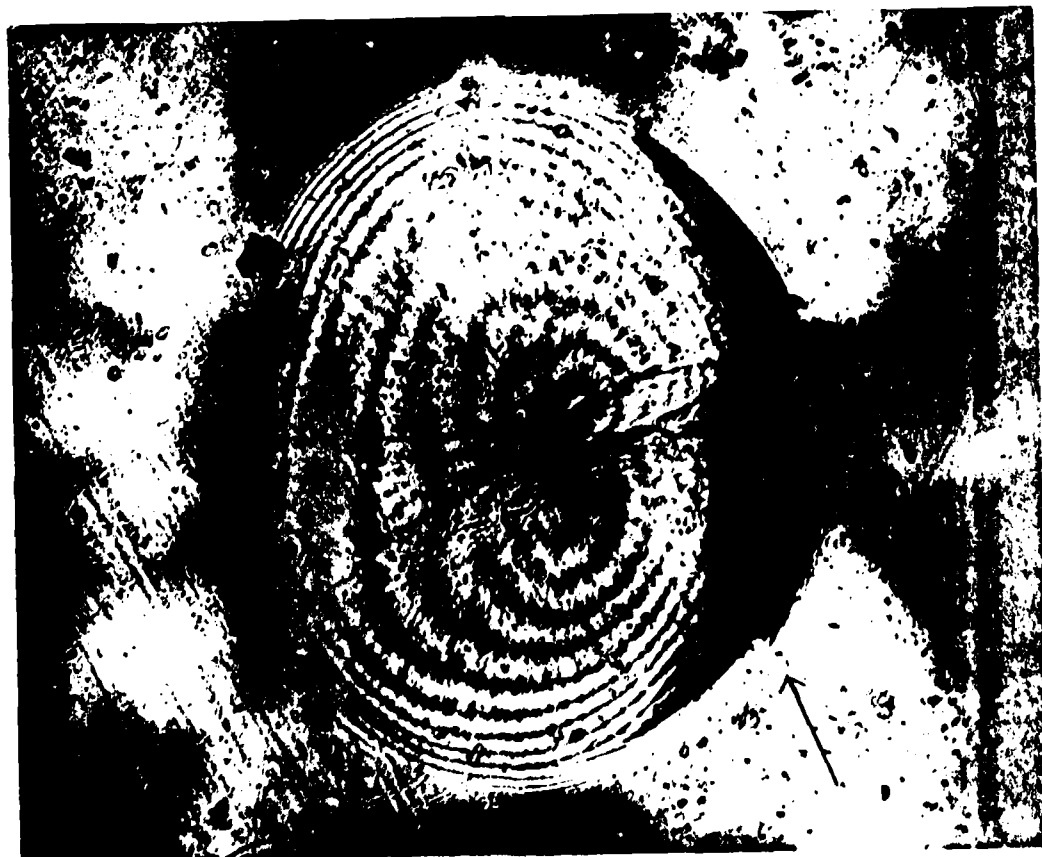
Figure 7(a)   Edge-on view of penny-shaped crack in polyester resin designated A in reference 1. The marker is 0.1 mm

(b)   Same crack after drying

Figure 8   Face-on views of penny-shaped cracks after drying. Notice the interference fringes. (a) epoxy, (b) polyester resin

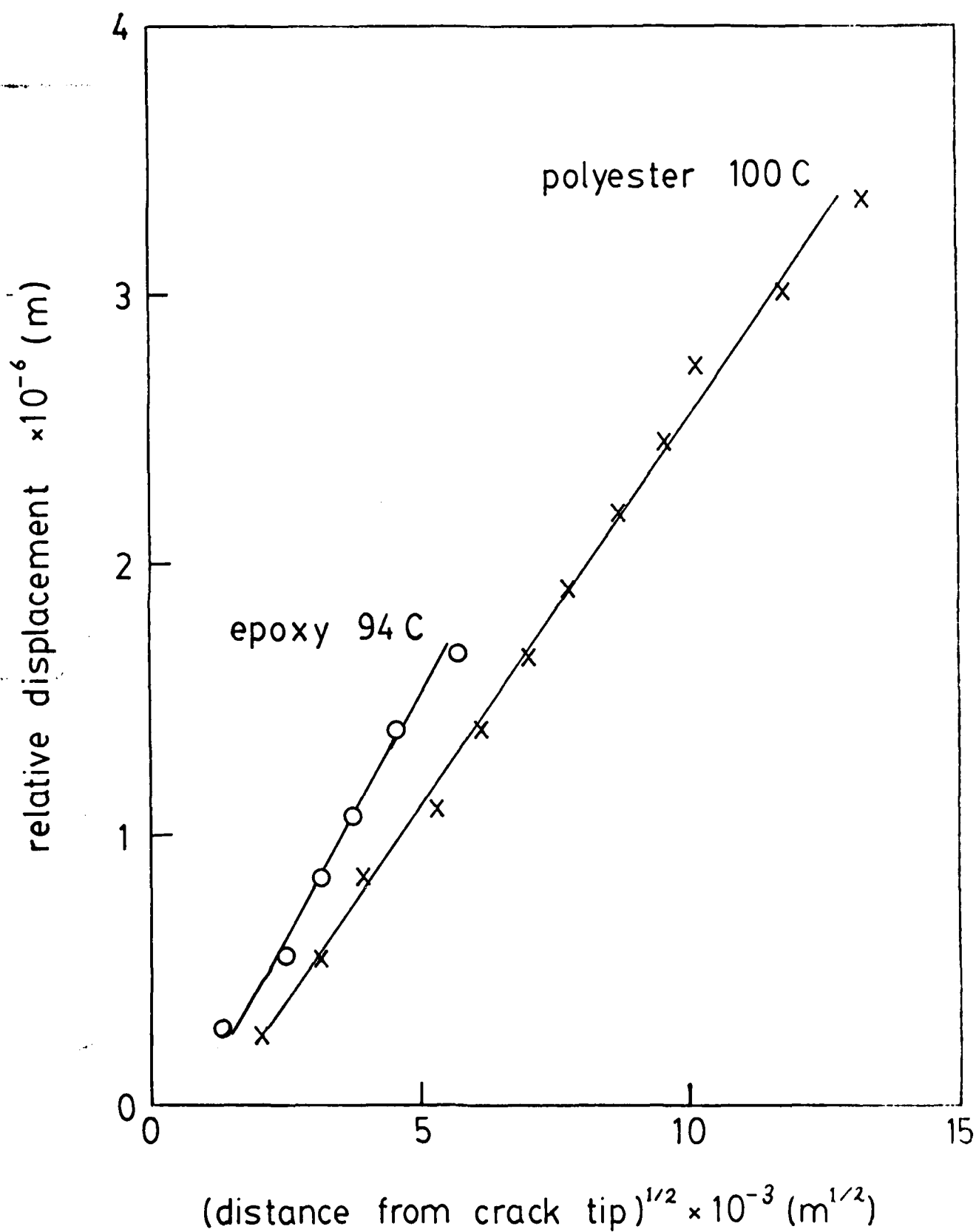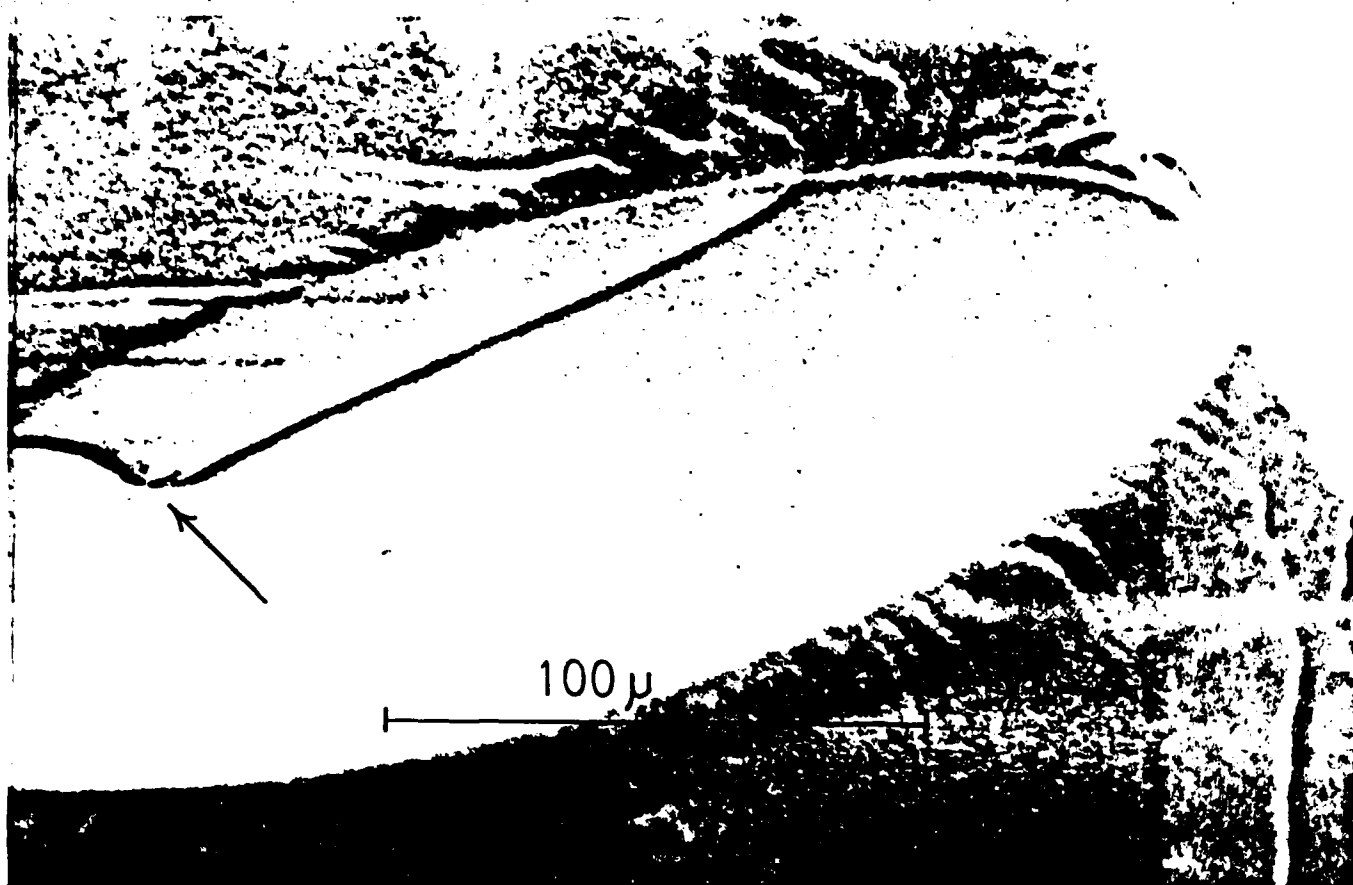Figure 9   Data from profiles of penny-shaped cracks after drying

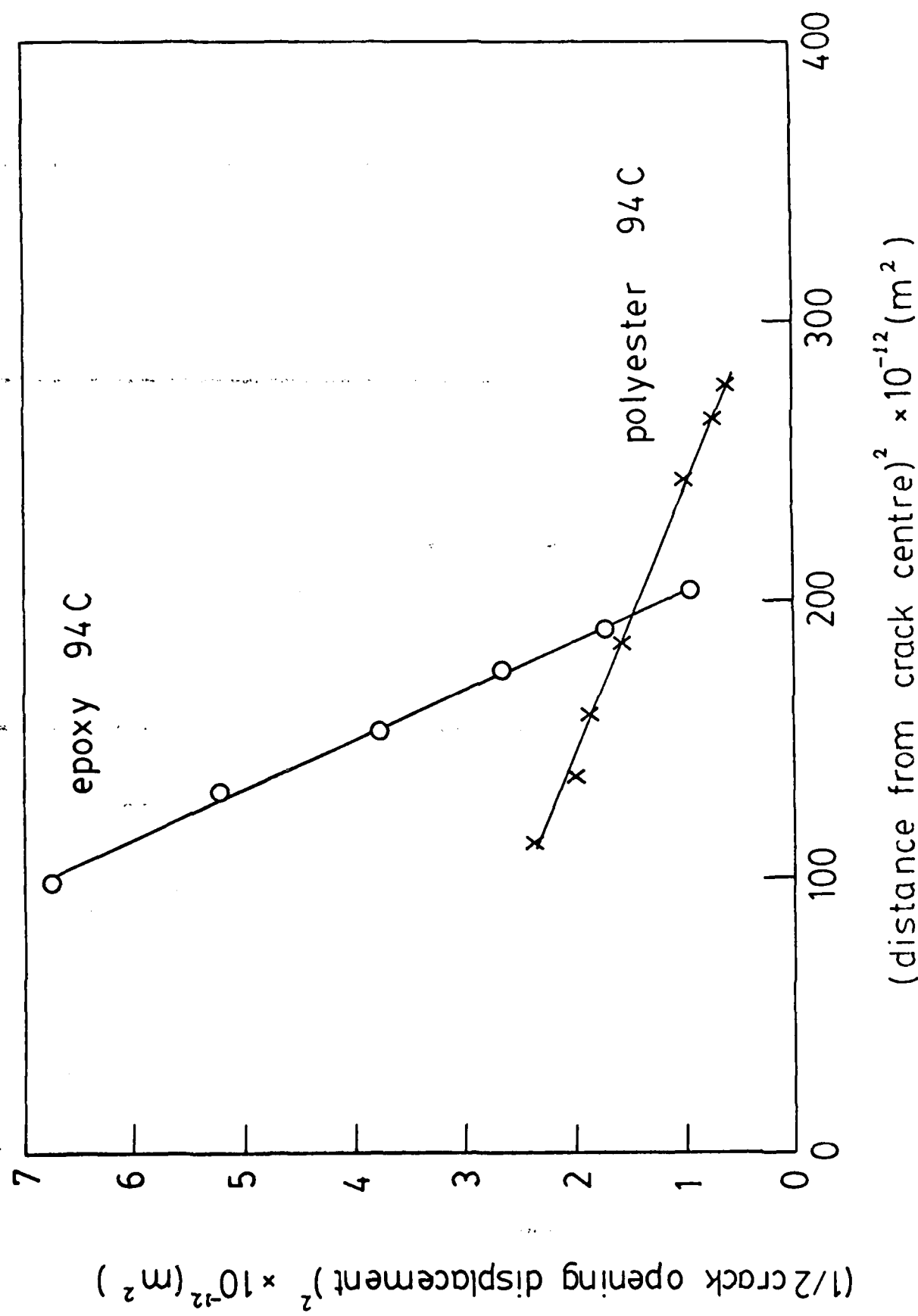Figure 10   Solute deposit on the surface of a penny-shaped crack in (a) epoxy resin (b) polyester resin

Figure 11 η_0^2 versus x^2 data from profiles of penny-shaped cracks in epoxy and polyester resin
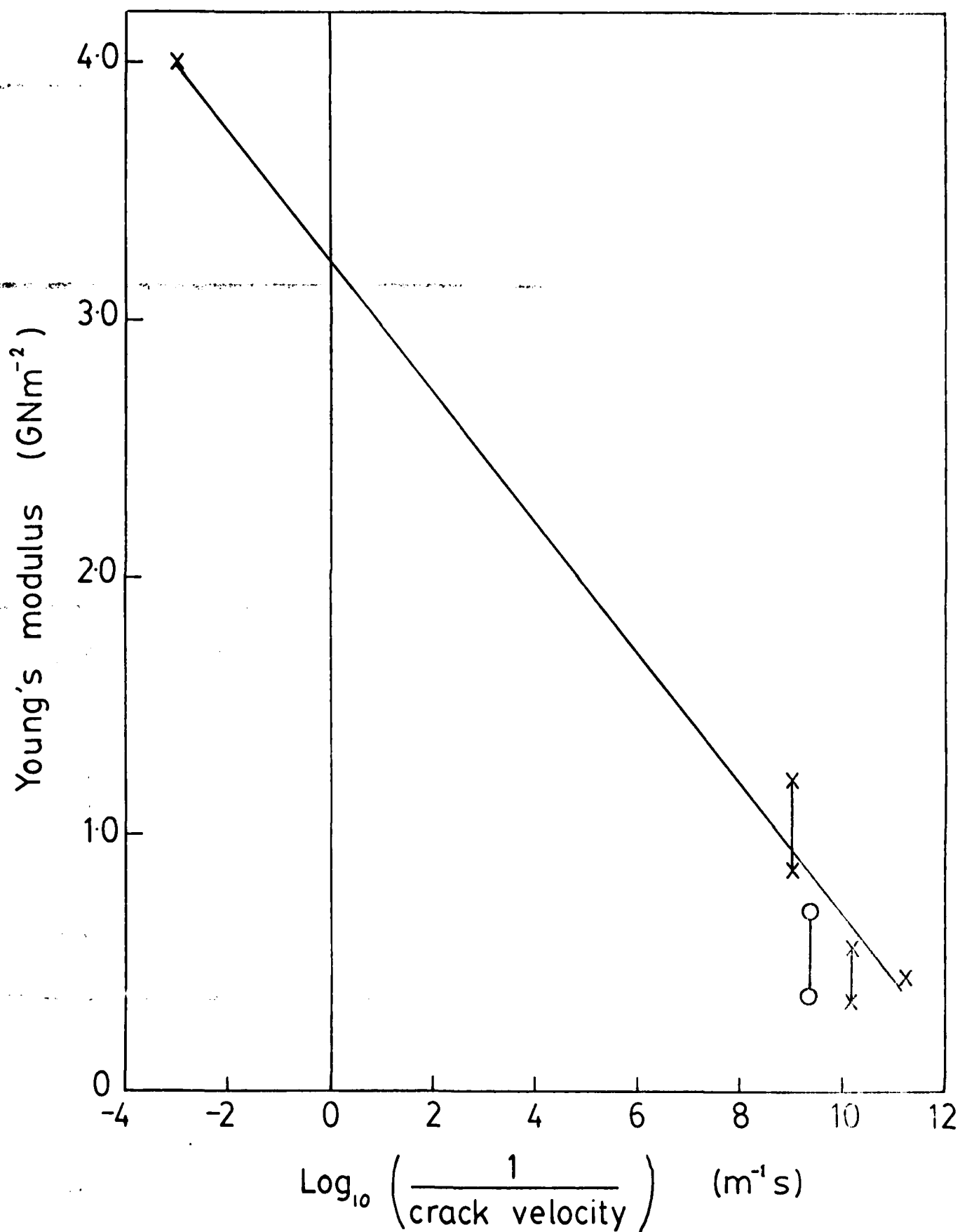
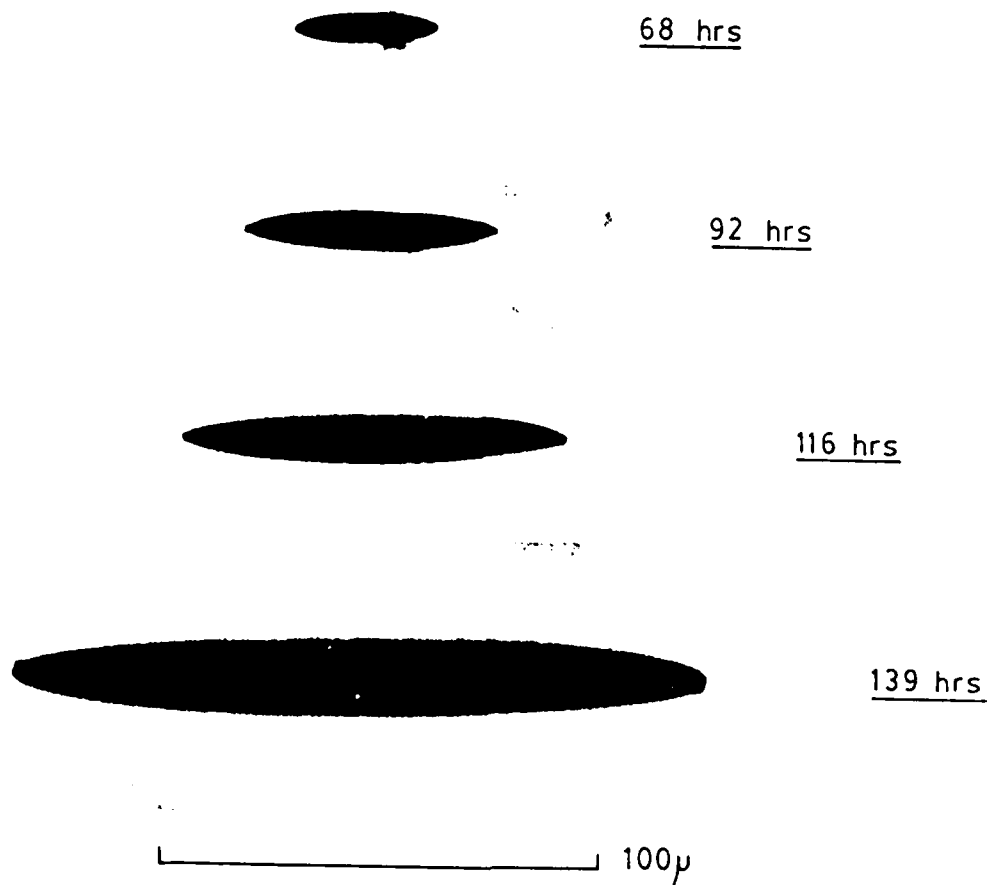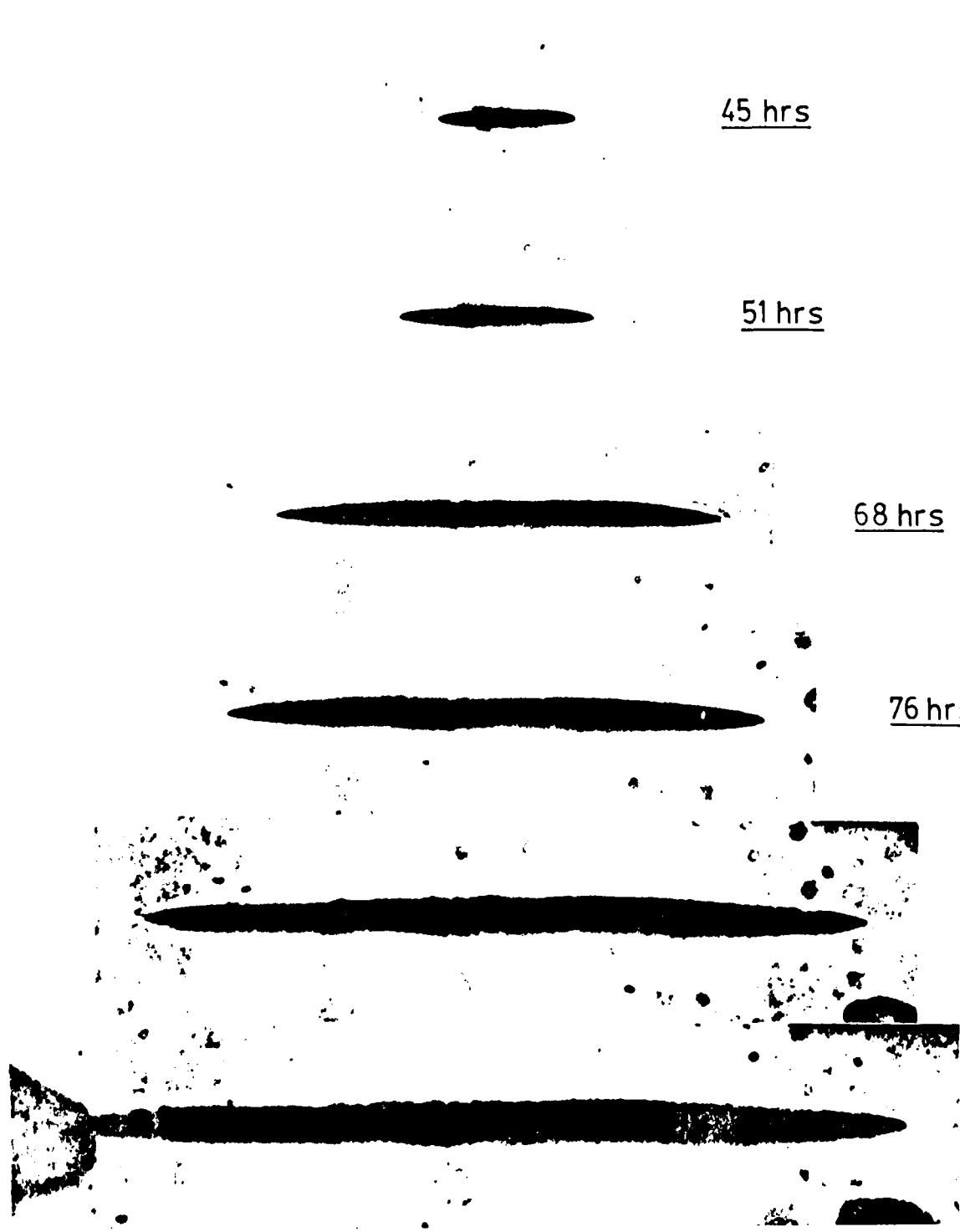Figure 12   Time (proportional to 1/crack velocity) dependence of Young's modulus for epoxy and polyester resins. Note the approximation to exponential behaviour

Figure 13(a)   Edge-on view of growth of single penny-shaped crack ~0.2mm below the surface in epoxy resin
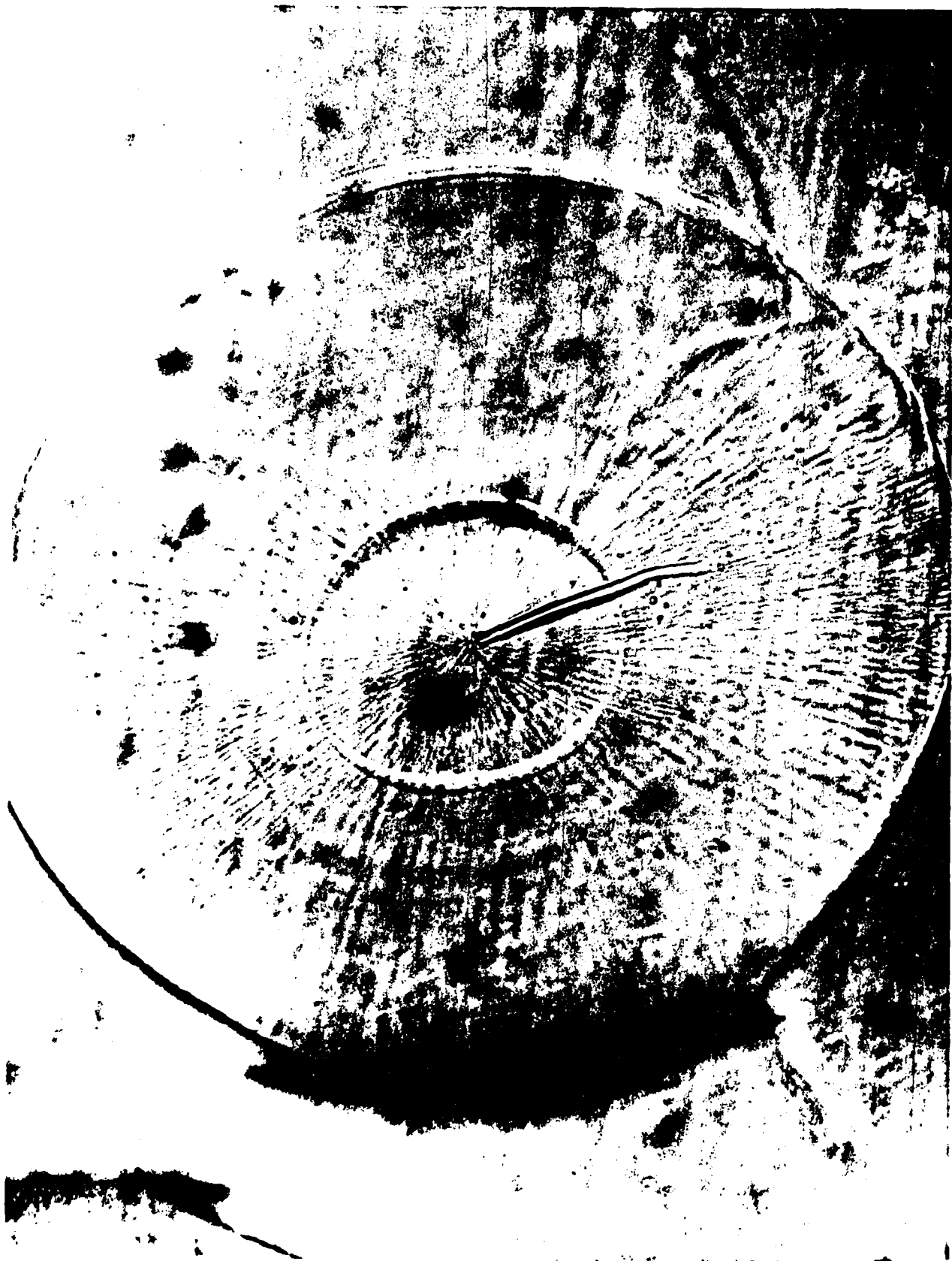
(b)   Same in polyester resin

Figure 14   Crack showing concentric growth ring structure

Figure 15   See text

Figure 16(a)   Locations of maximum tensile stress on an elliptic cavity in a plate subjected to biaxial tension

(b)   Crack propagation from one such location

Figure 17 Δv versus $r^{1/2}$ data for cracks grown in both epoxy and polyester resin at 94C

Figure 18   Crack velocity (v) versus stress intensity factor (K) for osmotic pressure filled cracks, $\bigcirc$ epoxy, $\times$ polyester resin

Figure 19   Scanning electron micrograph of E glass fibre etched during osmosis

Figure 20   Electron back scattering diffraction patterns from near (001) oriented α-quartz bonded to epoxy resin. The incident electron beam is further than $5\mu m$ from the interface in (a) and ~$2\mu m$ from the interface in (b)

Figure 21   High order Laue zone lines in convergent beam electron diffraction patterns from α-quartz bonded to epoxy resin. The distances from the interface are (a) $3\mu m$, (b) $1.3\mu m$ and (c) 800nm

Figure 22   Estimated angular spread of diffraction planes in the region of crystal samples in Figure 17

Figure 1   Resin cracks accompanying loss of load transfer in a C-glass/polyester composite, C-glass contains 9.6 wt% Na₂O. Specimen immersed in boiling water for 20 hrs.

Figure 2

Figure 3

Figure 4

Figure 5

Figure   2   Applied stress as a function of volume of a Griffith's crack
Figure   3   Crack volume vs internal pressure for an inflated crack
Figure   4   Energy vs volume of an inflated crack
Figure   5   Osmotic   pressure   vs   solute   concentration   for   some   common
             inorganic solutes

Figure 6(a) Penny-shaped crack in KCl-doped epoxy resin photographed edge-on. 140 hrs immmersion in water at 94C
(b) Same crack after drying in air for 1 hr at 100C
(c) Same as (b) with polarisers crossed. The flare of bright contrast is attributed partly to change of polarisation of light reflected by the crack faces and, more importantly, to permanent molecular orientation in resin immediately adjacent to the crack.

A

B

Figure 7(a) Edge-on view of penny-shaped crack in polyester resin
designated A in reference 1. The marker is 0.1 mm
(b) Same crack after drying

Figure 8   Face-on views of penny-shaped cracks after drying. Notice the interference fringes. (a) epoxy, (b) polyester resin

Figure 9   Data from profiles of penny-shaped cracks after drying

Figure 10   Solute deposit on the surface of a penny-shaped crack in (a) epoxy resin (b) polyester resin

Figure 11 n_o^2 versus x^2 data from profiles of penny-shaped cracks in epoxy and polyester resin

Figure 12 Time (proportional to 1/crack velocity) dependence of Young's modulus for epoxy and polyester resins. Note the approximation

68 hrs

92 hrs

116 hrs

139 hrs

⊢————————————————⊣ 100µ

Figure 13(a) Edge-on view of growth of single penny-shaped crack ~0.2mm
below the surface in epoxy resin

45 hrs

51 hrs

68 hrs

76 hrs

90 hrs

97 hrs

⊢————————⊣ 100μ

Figure 14   Crack showing concentric growth ring structure

Figure 15   See text
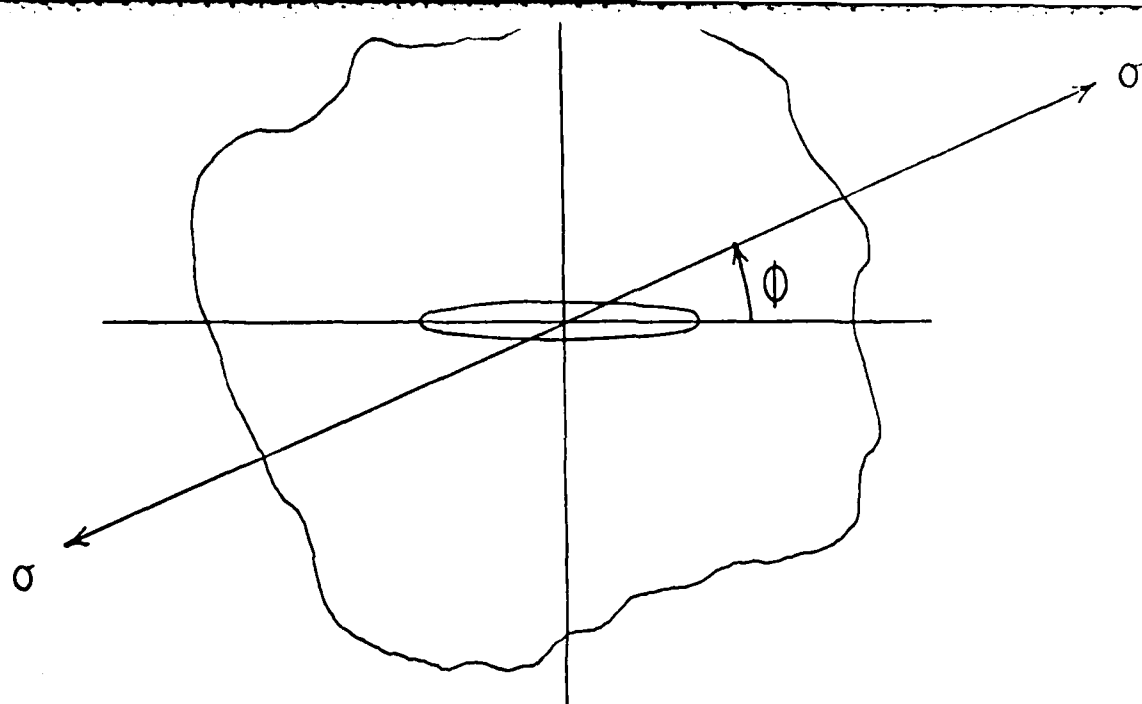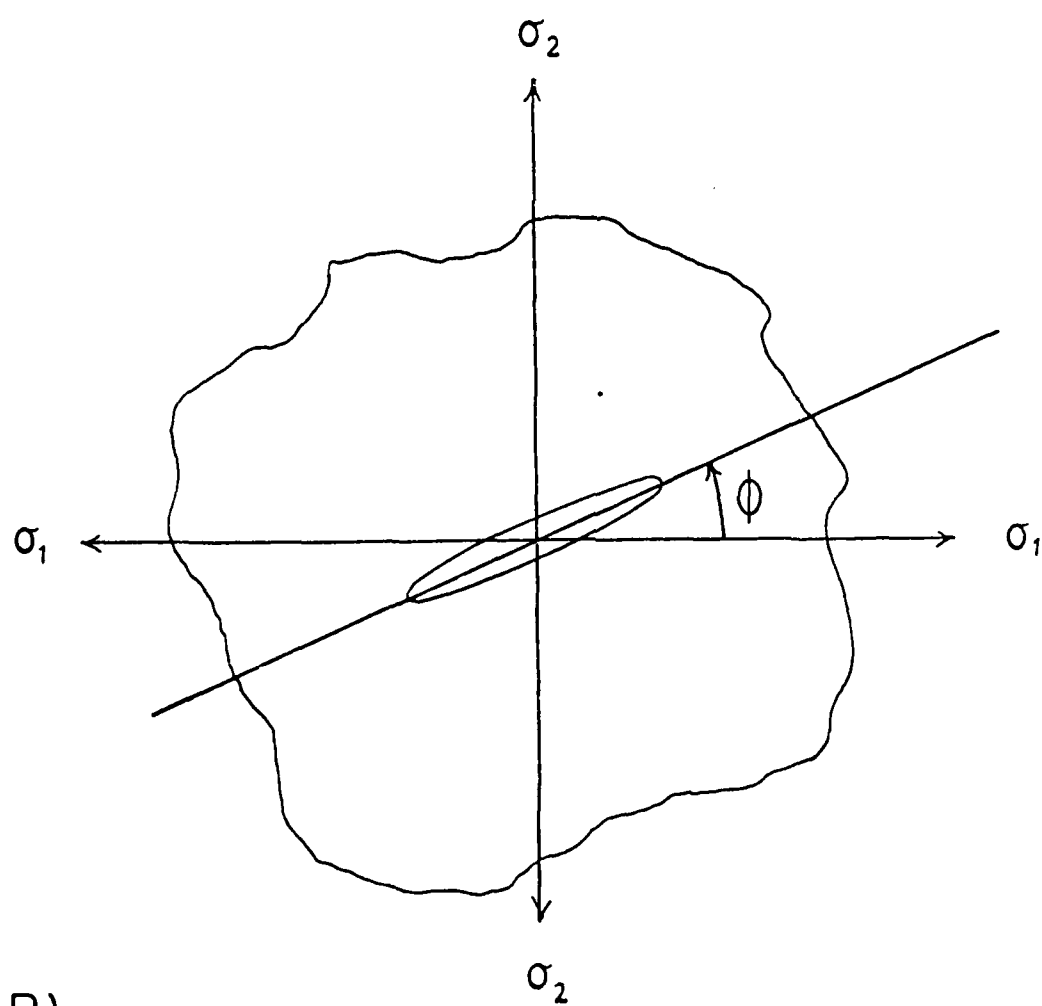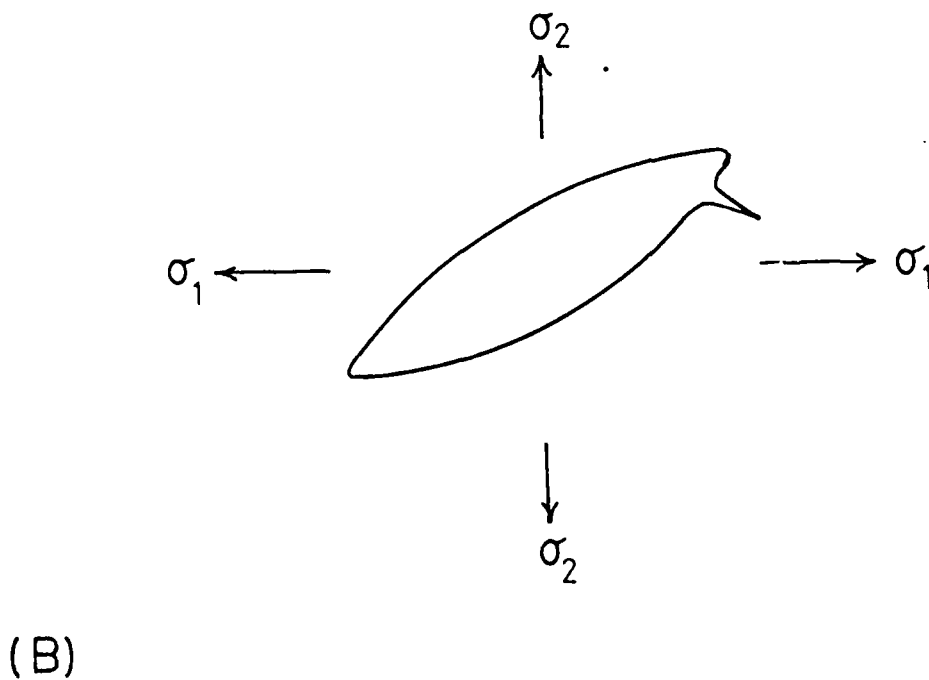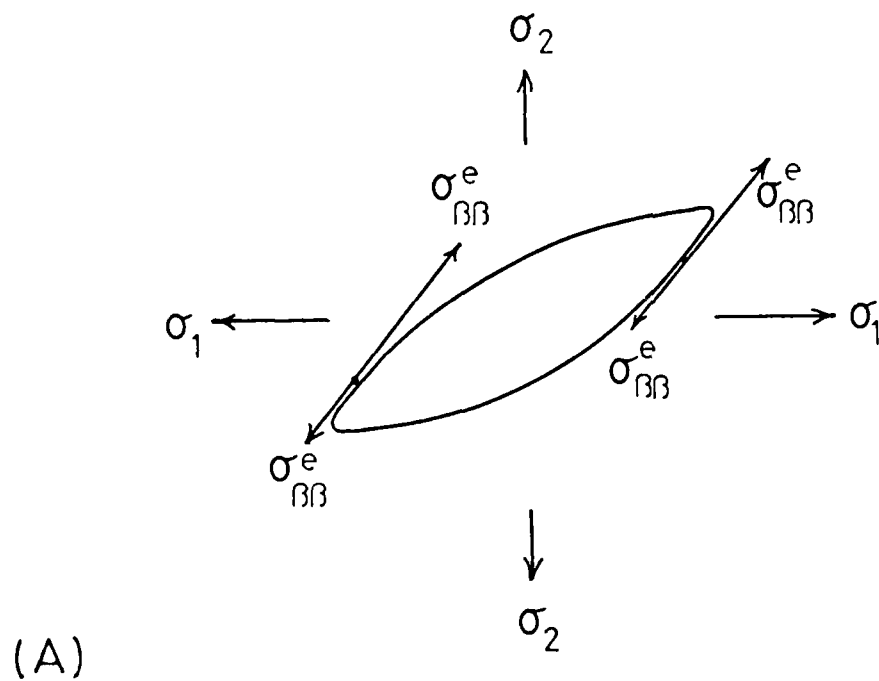
Figure 16(a) Locations of maximum tensile stress on an elliptic cavity in a
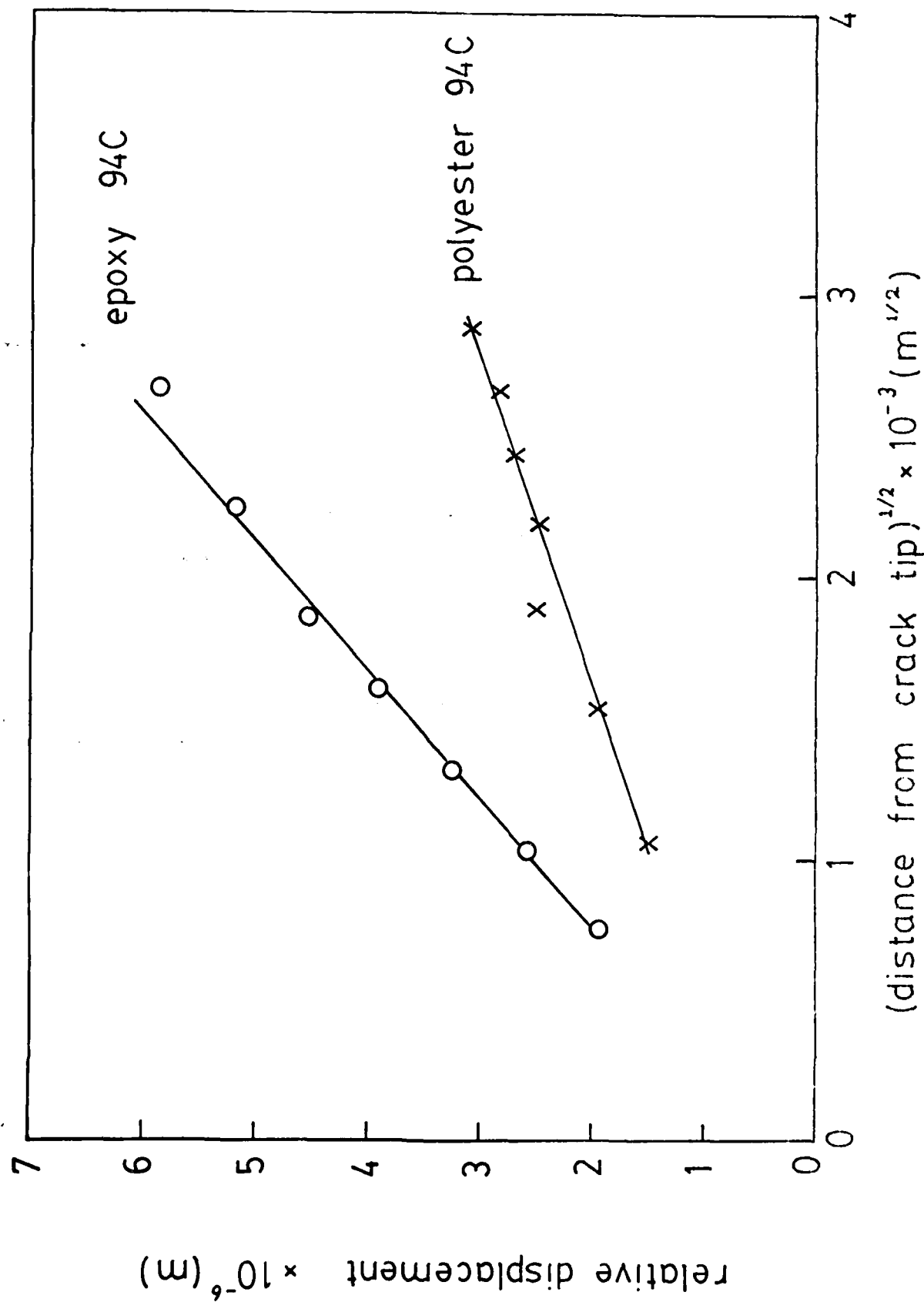
Figure 17   Δv versus $r^{1/2}$ data for cracks grown in both epoxy and polyester resin at 94C
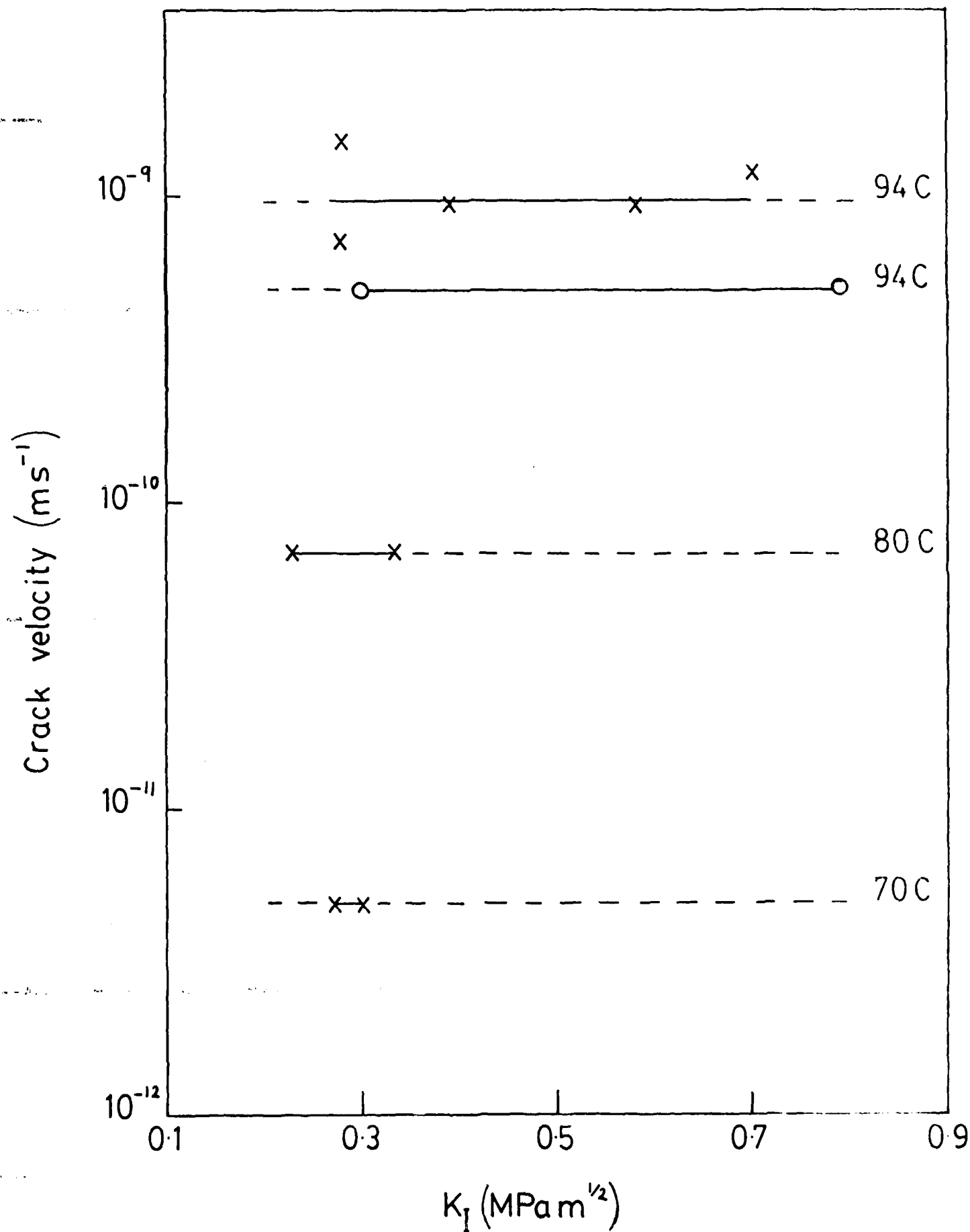
Figure 18 Crack velocity (v) versus stress intensity factor (K) for osmotic pressure filled cracks O epoxy X polyester resin

Figure 19   Scanning electron micrograph of E glass fibre etched during osmosis

a

b

Figure 20   Electron back scattering diffraction patterns from near (`001)
oriented α-quartz bonded to epoxy resin. The incident electron
beam is further than 5μm from the interface in (a) and ~2μm from
the interface in (b)
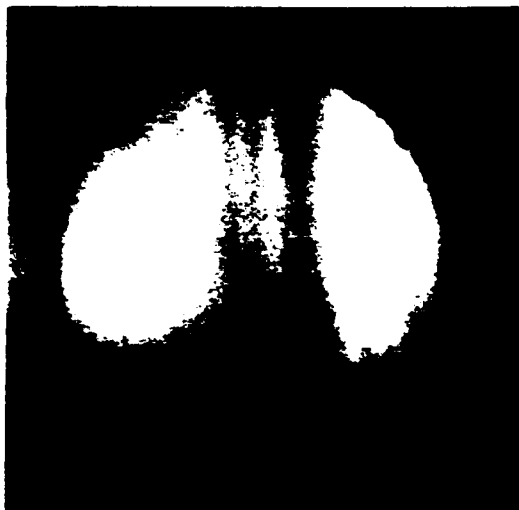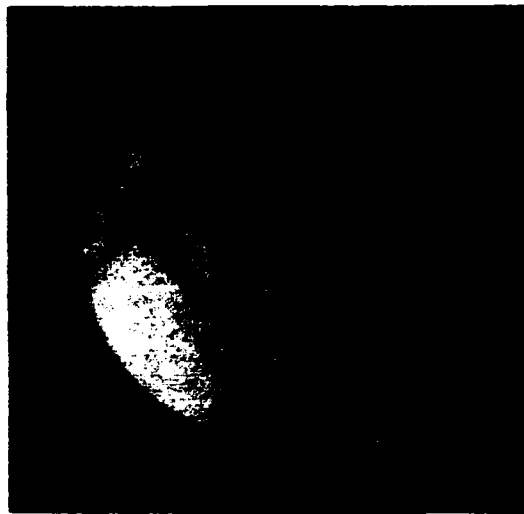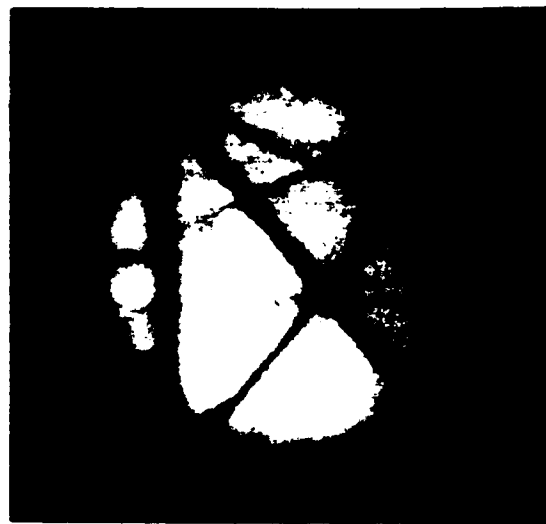
Figure 21   High order Laue zone lines in convergent beam electron diffraction patterns from α-quartz bonded to epoxy resin. The distances from the interface are (a) 3μm, (b) 1.3μm and (c) 800nm

Figure 22   Estimated angular spread of diffraction planes in the region of
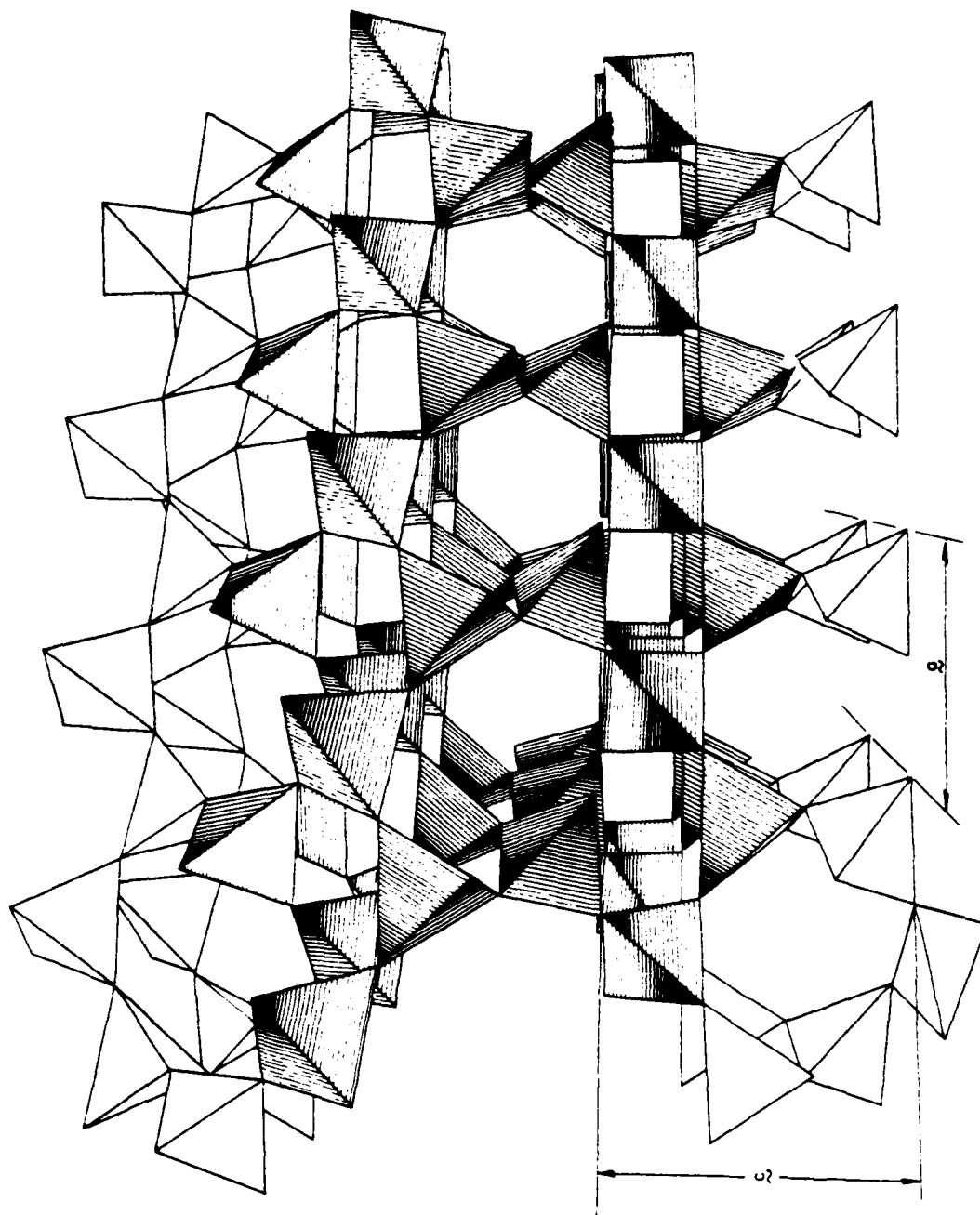crystal samples in Figure 17

Figure 23 SiO_2^{4-} tetrahedron model of α-quartz showing channels of corner sharing tetrahedra
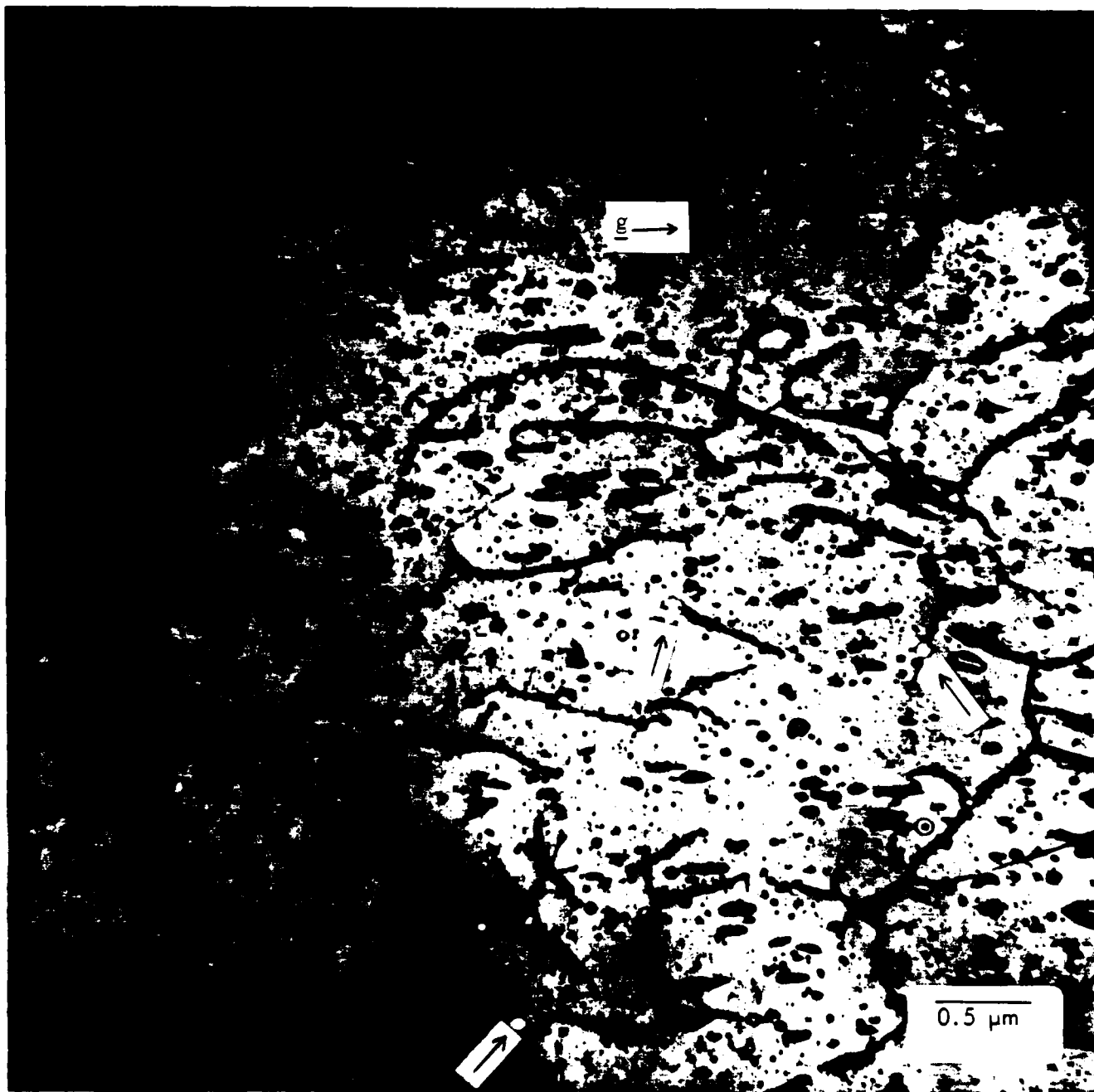
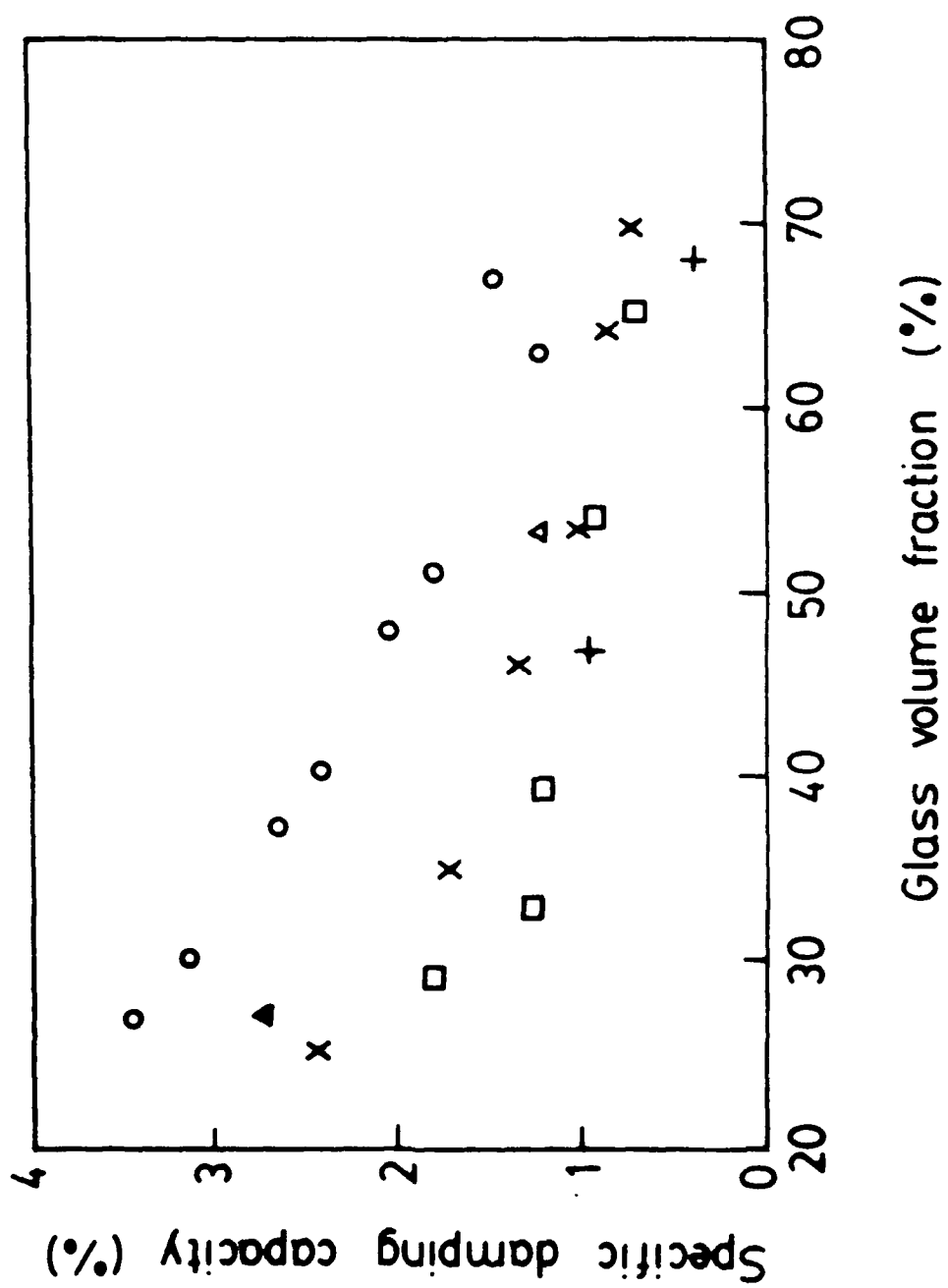Figure 24   Transmission electron micrograph of α-quartz

Figure 25   Dependence of mechanical damping on fibre/matrix interfacial area. Fibre diameters (μm): ○ 10, △ 20, × 30, □ 50, + 60

END

FILMED

9-83

DTIC